

1
2
3
4
5
6
7
8
9
10
11
12
13
14
15
16
17
18
19
20
21
22
23
24
25

Investigation of CATS aerosol products and application toward global diurnal variation of aerosols

Logan Lee¹, Jianglong Zhang¹, Jeffrey S. Reid², and John E. Yorks³

¹Department of Atmospheric Sciences, University of North Dakota, Grand Forks, ND

²Marine Meteorology Division, Naval Research Laboratory, Monterey, CA

³NASA Goddard Space Flight Center, Greenbelt, MD

Submitted to

ACP

Dec. 2018

Corresponding Author: jzhang@atmos.und.edu; logan.p.lee@und.edu

26
27
28
29
30
31
32
33
34
35
36
37
38
39
40
41
42
43
44

Abstract

We present a comparison of 1064 nm aerosol optical depth (AOD) and aerosol extinction profiles from the Cloud-Aerosol Transport System (CATS) Level 2 aerosol product with collocated Aerosol Robotic Network (AERONET) AOD, Aqua and Terra Moderate Imaging Spectroradiometer (MODIS) Dark Target AOD and Cloud-Aerosol Lidar with Orthogonal Polarization (CALIOP) AOD and extinction data for the period of Mar. 2015-Oct. 2017. Upon quality assurance checks of CATS data, reasonable agreement is found between aerosol data from CATS and other sensors. Using quality assured CATS aerosol data, for the first time, variations in AODs and aerosol extinction profiles are evaluated at 00, 06, 12, and 18 UTC (and/or 0:00 am, 6:00 am, 12:00 pm and 6:00 pm local solar times) on both regional and global scales. This study suggests that marginal variations are found in AOD from a global mean perspective, with the minimum aerosol extinction values found at 6:00 pm (local time) near the surface layer for global oceans, for both the June-November and December-May seasons. Over land, below 500m, the daily minimum and maximum aerosol extinction values are found at 12:00pm and 00:00/06:00 am (local time), respectively. Strong diurnal variations are also found over North Africa and India for the December-May season, and over North Africa, South Africa, Middle East, and India for the June-November season.

45 **1.0 Introduction**

46 Aerosol measurement through the sun-synchronous orbits of Terra and Aqua by nature
47 encourages a larger scale, daily average point of view. Yet, we know that pollution (e.g., Zhao et
48 al., 2009; Tiwari et al., 2013; Kaku et al., 2018), fires and smoke properties (e.g., Reid et al., 1999;
49 Giglio et al., 2003; Hyer et al., 2013), and dust (e.g., Mbourou, et al., 1997; Fiedler et al., 2013;
50 Heinold et al., 2013) can exhibit strong diurnal behavior. Sun-synchronous passive satellite
51 aerosol observations from the solar spectrum only provide a small sampling of the full diurnal
52 cycle. Geostationary sensors such as the Advanced Himawari Imager (AHI) on Himawari 8
53 (Yoshida et al., 2018) and Advanced baseline Imager on GOES-16/17 (Aerosol Product
54 Application Team of the AWG Aerosols/Air Quality/Atmospheric Chemistry Team, 2012)
55 satellites, while an improvement over their predecessors, must overcome the broader range of
56 scattering and zenith angles (Wang et al., 2003; Christopher and Zhang, 2002) with no nighttime
57 retrievals. AEROSOL ROBOTIC NETWORK (AERONET; Holben et al., 1998) based sun photometer
58 studies improve sampling, but until very recently with the development of a prototype lunar
59 photometry mode, are also limited to daylight hours. The critical early morning and evening are
60 largely missed in solar observation-based approaches.

61 Observations of the diurnal variations of aerosol properties are needed for improving
62 chemical transport modeling, geochemical cycles and ultimately climate. The measurement of
63 diurnal variations of aerosol properties resolved in the vertical is especially crucial for visibility
64 and particulate matter forecasts. Indeed, the periods around sunrise and sunset show significant
65 near surface variability that is difficult to detect with passive sensors. While lidar data from Cloud-
66 Aerosol Lidar with Orthogonal Polarization (CALIOP) provide early afternoon and morning

67 observations, two temporal points and a 16-day repeat cycle are insufficient to evaluate the critical
68 morning and evening hours where many key aerosol lifecycle processes take place.

69 Some of the limiting factors in previous studies can be addressed by the Cloud-Aerosol
70 Transport System (CATS) lidar that flew aboard the International Space Station (ISS) from 2015
71 to 2017 (McGill et al. 2015). The ISS's precessing orbit with a 51.6° inclination allows for 24
72 hour sampling of the tropics to mid-latitudes, with the ability to observe aerosol and cloud vertical
73 distributions at both day and night time with high temporal resolution. For a given location within
74 $\pm 51.6^\circ$ (Latitude), after aggregating roughly 60 days of data, near full diurnal cycle of aerosol and
75 cloud properties can be obtained from CATS observations (Yorks et al. 2016). This provides a
76 new opportunity for studying diurnal variations (day and night) in aerosol vertical distributions
77 from space observations.

78 Use of CATS has its own challenges. Most importantly, CATS retrievals must cope with
79 variable solar noise around the solar terminator where we expect some of the strongest diurnal
80 variability to exist. Further, CATS lost its 532 nm channel early in its deployment, leaving only a
81 1064 nm channel functioning. The availability of only one wavelength limited the CATS cloud-
82 aerosol discrimination algorithm, which can cause a loss of accuracy compared to CALIPSO
83 which has 2 wavelengths. This deficiency is in part overcome by using the Feature Type Score
84 (CATS Algorithm Theoretical Basis Document). Using two years of observations from CATS, in
85 this paper, we focus on understanding of the following questions: How well do CATS derived
86 aerosol optical depth (AOD) and aerosol vertical distributions compare with aerosol properties
87 derived from other ground-based and satellite observations such as AERONET, MODIS and
88 CALIOP? Do differences exhibit a diurnal cycle? What are the diurnal variations of aerosol optical

89 depth on a global domain? What are the diurnal variations of aerosol vertical distribution on both
90 regional and global scales?

91

92 **2.0 Datasets**

93 Four datasets, including ground-based AERONET data, as well as satellite retrieved
94 aerosol properties from MODIS and CALIOP, are used for inter-comparing with AOD and aerosol
95 vertical distributions from CATS. Upon thorough evaluation and quality assurance procedures,
96 CATS data are further used for studying diurnal variations of AOD and aerosol vertical
97 distributions for the period of Mar. 2015 – Oct. 2017.

98

99 **2.1 CATS**

100 CATS Level 2 (L2) Version 3-00 5 km Aerosol Profile products (L2O_D-M7.2-V3-
101 00_05kmPro, L2O_N-M7.2-V3-00_05kmPro) were used in this study for nearly the entire period
102 of CATS operation on the ISS (~Mar. 2015–Oct. 2017). CATS L2 profile data is provided at 5
103 km along-track horizontal resolution and 533 vertical levels at 60 m vertical resolution and a
104 wavelength of 1064 nm. CATS also provides data at 532 nm, but due to a laser-stabilization issue,
105 532 nm data is not recommended for use (Yorks et al. 2016). Thus, only 1064 nm products were
106 used in this study. Although the uncertainties in CATS aerosol retrievals have not yet been
107 documented for the CATS V3-00 extinction and AOD products, much like CALIOP, uncertainties
108 in the calibration and assumed lidar ratios are the primary contributors to the extinction and AOD
109 uncertainties. The uncertainties in the CATS 1064 nm attenuated total backscatter (ATB) is on the
110 order of 7-10% for nighttime and is around 20% for daytime (Pauly et al., 2019), while the
111 uncertainties in the assumed 1064 nm lidar ratios for CATS are 30%. Thus, the CATS 1064 nm

112 extinction (40-70%) and AOD (30-50%) uncertainties are very similar to the corresponding
113 CALIOP 1064 nm uncertainties.

114 CATS data are quality-assured following a manner similar to Campbell et al. (2012), which
115 was applied to CALIOP. QA thresholds (including extinction QC flag, Feature Type Score, and
116 uncertainty in extinction coefficient) are listed below:

117 (a) Extinction_QC_Flag_1064_Fore_FOV is equal to 0 (non-opaque layer; lidar ratio
118 unchanged)

119 (b) Feature_Type_Fore_FOV = 3 (contains aerosols only)

120 (c) $-10 \leq \text{Feature_Type_Score_FOV} \leq -2$ (Feature Type Score < 0 is aerosol, with -10
121 being complete confidence, and 0 being as likely to be cloud as aerosol)

122 (d) $\text{Extinction_Coefficient_Uncertainty_1064_Fore_FOV} \leq 10 \text{ km}^{-1}$

123 Extinction was also constrained using a threshold as provided in the CATS data catalog
124 ($\text{Extinction_Coefficient_1064_Fore_FOV} \leq 1.25 \text{ km}^{-1}$), similar to several previous studies
125 (Redemann et al., 2012; Toth et al., 2016). Only profiles with extinction coefficient values less
126 than 1.25 km^{-1} are included in this study. Small negative extinction coefficient values, however,
127 are included in aerosol profile related analysis, to reduce potential high biases in computed mean
128 profiles. Note that a similar approach has also been conducted in deriving passive-based AOD
129 climatology (e.g. Remer et al., 2005). For this study, both the
130 $\text{Aerosol_Optical_Depth_1064_Fore_FOV}$ and $\text{Extinction_Coefficient_1064_Fore_FOV}$ datasets
131 were used to provide AOD and 1064 nm extinction profiles (hereafter the term “extinction” will
132 refer to 1064 nm unless explicitly stated otherwise), respectively.

133

134 **2.2 CALIOP**

135 NASA's CALIOP is an elastic backscatter lidar that operates at both 532 nm and 1064 nm
136 wavelengths (Winker et al., 2009). Being a part of the A-Train constellation (Stephens et al.,
137 2002), CALIOP provides both day- and night-time observations of Earth's atmospheric system, at
138 a sun-synchronous orbit, with a laser spot size of around 70 m and a temporal resolution of ~16
139 days (Winker et al., 2009). For this study, CALIOP Level 2.0 Version 4.1 5 km Aerosol Profile
140 products (L2_05kmAProf) are used for inter-comparing to CATS retrieved AODs and aerosol
141 vertical distributions.

142 L2_05kmAProf data are available at 5 km horizontal resolution along-track and include
143 aerosol retrievals at both 532 nm and 1064 nm wavelengths. The vertical resolution is 60 m near-
144 surface, degrading to 180 m above 20.2 km in MSL altitude. As only 1064 nm CATS data are
145 used in this study as mentioned above, likewise only those CALIOP parameters relating to 1064
146 nm are used in this study (Vaughan et al., 2019; Omar et al., 2013). Note that as suggested by
147 Rajapakshe et al. (2017), lower signal-to-noise ratio (SNR) and higher minimum detectable
148 backscatter are found for the CALIOP 1064 nm data in-comparing with the CALIOP 532 nm data.
149 Also, the CALIOP aerosol layers are detected at 532 nm and the 1064 nm extinction is only
150 computed for the bins within these layers. This may introduce a bias for aerosol above cloud
151 studies. The uncertainties in retrieved aerosol extinction, as suggested by Young et al., (2013), is
152 around 0.05–0.5 km⁻¹ for the 532 nm channel. Validated against AERONET data, Omar et al.,
153 (2013) suggested that 74% and 81% of the CALIOP AOD retrievals fall within the expected
154 uncertainties (0.05+0.4*AOD) as suggested by Winker et al., (2009) for the 1064nm channel, for
155 all sky and clear sky conditions respectively.

156 In this study, Extinction_Coefficient_1064 and
157 Column_Optical_Depth_Tropospheric_Aerosols_1064 are used for CALIOP extinction and AOD

158 retrievals, respectively (Vaughan et al., 2019; Omar et al., 2013). As with the CATS data, CALIOP
159 data are quality-assured following the quality assurance steps as mentioned in a few previous
160 studies (e.g. Campbell et al., 2012; Toth et al., 2016; 2018). These QA thresholds are listed below:

161 (a) Extinction_QC_Flag_1064 is equal to 0 (unconstrained retrieval; initial lidar ratio
162 unchanged)

163 (b) Atmospheric_Volume_Description = 3 or 4 (contains aerosols only)

164 (c) $-100 \leq \text{CAD_Score} \leq -20$ (CAD < 0 is aerosol, with -100 being complete confidence,
165 and 0 being as likely to be cloud as aerosol)

166 (d) Extinction_Coefficient_Uncertainty_1064 $\leq 10 \text{ km}^{-1}$

167 Furthermore, as in Campbell et al. (2012), only those profiles with AOD > 0 were retained
168 in order to avoid profiles composed of only retrieval fill values. Extinction was also constrained
169 to the nominal range provided in the CALIOP data catalog (Extinction_1064 $\leq 1.25 \text{ km}^{-1}$), similar
170 to our QA procedure for CATS as described above.

171

172 **2.3 MODIS Collection 6.1 Dark Target product**

173 Moderate Resolution Imaging Spectroradiometer (MODIS) Aqua and Terra Collection 6.1
174 Dark Target over-ocean AOD data (Levy et al., 2013) were used for comparison to CATS AOD.
175 The data field of “Effective_Optical_Depth_Best_Ocean” was used and only those data flagged as
176 “good” or “very good” by the Quality_Assurance_Ocean runtime QA flags were selected for this
177 study, similar to Toth et al. (2018). Because MODIS does not provide AOD in the 1064 nm
178 wavelength, AOD retrievals from 860 and 1240 nm spectral channels are used to logarithmically
179 interpolate AODs at 1064 nm. Here we assume the Ångström Exponent value, computed using
180 instantaneous AOD retrievals at the 860 and 1240 nm, remains the same for the 860 to 1064 nm

181 wavelength range, similar to what has been suggested by Shi et al., (2011; 2013). Mean and
182 standard deviation of Ångström exponents using this method were 0.69 and 0.55, respectively.
183 Only totally cloud free (or cloud fraction equal to zero) retrievals, as indicated by the
184 Cloud_Fraction_Land_Ocean parameter, are used. While the uncertainties in MODIS infrared
185 (e.g. 1240 nm) retrievals are less explored, the reported over ocean MODIS DT AOD retrievals
186 are $(+(0.04 + 0.1 \cdot \text{AOD}), -(0.02 + 0.1 \cdot \text{AOD}))$ for the green channel (Levy et al., 2013).

187

188 **2.4 AERONET**

189 By measuring direct and diffuse solar energy, AERONET observations are used for
190 retrieving AOD and other ancillary aerosol properties such as size distributions (Holben et al.,
191 1998). AERONET data are considered as the ground truth for evaluating CATS retrievals in this
192 study. Only cloud screened and quality assured version 3 level 2 AERONET data at the 1020 nm
193 spectrum are selected and are used for inter-comparing with CATS AOD retrievals at the 1064 nm
194 wavelength. AERONET does not have specific guidance on error in the 1020 nm channel, as it
195 is known to have some thermal sensitivities. However, they do report significantly more
196 confidence in version 3 of the data, which has temperature correction (Giles et al., 2019). Error
197 models are ongoing, and for this study we assume double the RMSE, or ± 0.03 . Note that Version
198 3 AERONET data are designed to reduce thin cirrus cloud contamination as well as rescue heavy
199 aerosol scenes that were misclassified as clouds in previous versions (e.g. Giles et al., 2019).

200

201 **3.0 Results & Discussion**

202 **3.1 Inter-comparison of CATS data with AERONET, MODIS and CALIOP data**

203 Note that most evaluation efforts for passive and active sensor AOD retrievals are focused
204 on the visible spectrum and the performance of AOD retrievals at the 1064 nm channel is less
205 explored. Thus, in this sub-section, the performance of over land and over ocean CATS AOD
206 retrievals are compared against AERONET and C6.1 over ocean MODIS Dark Target (DT)
207 aerosol products. In AOD related studies, CATS and CALIOP reported AOD values are used.
208 However, only AOD values with corresponding aerosol vertical extinction that meet the QA
209 criteria as mentioned in Sections 2.1 and 2.2 were used. CATS derived aerosol extinction vertical
210 distributions are also cross-compared against collocated CALIOP aerosol extinction vertical
211 distributions.

212

213 **3.1.1 CATS-AERONET**

214 As the initial check, CATS data from nearly the entire mission (Mar. 2015-Oct. 2017) were
215 spatially (within 0.4 degree Latitude and Longitude) and temporally (± 30 minutes) collocated
216 against ground-based AERONET data. Note that one AERONET measurement may be associated
217 with several CATS retrievals in both space and time, and vice versa. Thus, both CATS and
218 AERONET data were further averaged spatially and temporally, which results in only one pair of
219 collocated and averaged CATS and AERONET data for a given collocated incident. Also, only
220 data pairs with AOD larger than 0 from both instruments are used for the analysis. This step is
221 necessary to exclude CATS profiles with all retrieval fill values as discussed in Section 2 (Toth et
222 al., 2018). Such profiles containing all retrieval fill values were found to make up approximately
223 5.3% of all CATS profiles in the dataset. Note that the CATS-AERONET comparisons are for
224 daytime only, and higher uncertainties are expected for CATS daytime than nighttime AODs.

225 As shown in Figure 1a, without quality-assurance procedures, high spikes in CATS AOD
226 of above 1 (1064 nm) can be found for collocated AERONET data with AOD less than 0.4 (1020
227 nm). Still, those high spikes in CATS AOD are much reduced compared to the V2-01 CATS
228 aerosol products (e.g. a similar plot as Figure 1 is included in the Appendix A with the use of V2-
229 01 CATS aerosol data). Upon completion of the QA steps as outlined in Section 2.1, a reasonable
230 agreement is found between quality-assured CATS (1064 nm) vs. AERONET (1020 nm) AODs
231 with a correlation of 0.65 (Figure 1b). Comparing Figure 1a with 1b, with the loss of only ~1-2%
232 of collocated pairs due to the QA procedures, we have observed an overall improvement in
233 correlation between CATS and AERONET AOD from 0.51 to 0.64, thus, only QAed CATS data
234 are used hereafter. We also found that requiring the Extinction QC flag to be equal to 0 and the
235 Extinction Uncertainty to be less than 10 km^{-1} had the largest impacts on reducing the difference
236 in mean and medians of the AERONET and CATS AOD. Still, this exercise highlights the need
237 for careful quality checks of the CATS data before applying the CATS data for advanced
238 applications to overcome cloud-aerosol discrimination uncertainties.

239

240 **3.1.2 CATS-MODIS**

241 To examine over ocean performance, column integrated CATS AODs are inter-compared
242 with collocated Terra and Aqua C6.1 MODIS DT over ocean AOD, interpolated to 1064 nm. Over
243 ocean C6.1 MODIS DT data are selected due to the fact that higher accuracies are reported for
244 over ocean versus over land MODIS DT AOD retrievals (Levy et al., 2013). In addition, compared
245 to over land MODIS DT data, which provide AOD retrievals at three discrete wavelengths (0.46,
246 0.55 and 0.65 μm), over water AOD retrievals are available from 7 wavelengths including the 0.87
247 and 1.24 μm spectral channels, allowing a comparison with CATS AOD at the same wavelength

248 upon logarithmic interpolation, again, assuming the aerosol Ångström Exponent value remains
249 unchanged from 0.87 to 1.064 μm as well as from the 1.064 μm to 1.24 μm spectral channels.

250 MODIS and CATS AOT retrievals are collocated for the study period of Mar. 2015-Oct.
251 2017 (Figure 2). Pairs of CATS and MODIS data were first selected for both retrievals that fall
252 within ± 30 minutes and 0.4 degrees latitude and longitude of each other. Then, similar to the
253 AERONET and CATS collocation procedures, collocated pairs were further averaged to construct
254 one pair of collocated MODIS and CATS data for a given collocation incident. Shown in Figure
255 2a, a correlation of 0.72 is found between collocated over water Terra MODIS C6.1 DT and CATS
256 AODs with a slope of 0.74. Similar results are found for the comparisons between over water
257 Aqua MODIS and CATS AODs with a correlation of 0.74 and a slope of 0.70.

258

259 **3.1.3 CATS-CALIOP AOD**

260 In the previous two sections, AODs from CATS were inter-compared with retrievals from
261 passive-based sensors such as MODIS and AERONET. In this section, AOD data from CALIOP,
262 which is an active sensor, are evaluated against AOD retrievals from CATS. Note that despite
263 difference in instrumental designs, CALIOP and CATS are both elastic backscatter lidars. Again,
264 for each collocation incident, pairs of CALIOP and CATS data are selected in which both retrievals
265 fall within ± 30 minutes temporally and 0.4 degrees latitude and longitude spatially. There could
266 be multiple CATS retrievals corresponding to one CALIOP data point, and vice versa. Thus, the
267 collocated pairs are further averaged in such a way that only one pair of collocated CATS and
268 CALIOP data is derived for each collocation incident. .

269 Figure 3a shows the comparison of CATS and CALIOP AODs for all collocated pairs
270 including both day- and night-time. A reasonable correlation of 0.74, with a slope of 0.73, is found

271 for a total of 2762 collocated data pairs. Further breaking down the comparison into day and night
272 cases, a much better agreement is found between the two datasets during nighttime with
273 correlations of 0.81 and 0.83 for over-ocean and over-land cases respectively. In comparison, a
274 lower correlation of 0.64, with a slope of 0.49, is found between the two datasets, using over land
275 daytime data only, for a total of 170 collocated pairs. Correspondingly, a lower correlation of
276 0.55, with a slope of 0.57, is found between the two datasets, using over ocean daytime data only,
277 for a total of 1180 collocated pairs. This result is not surprising as daytime data from both CALIOP
278 and CATS are noisier due to solar contamination (e.g. Omar et al., 2013; Toth et al., 2016).

279 Note that based on the slopes of the regression lines shown in Figures 1-3, AODs retrieved
280 by CATS are less than AERONET, CALIOP and DT Aqua MODIS AOD retrievals. As shown
281 in Table 1, however, for the one-to-one collocated datasets, mean CATS AODs (1064 nm) are
282 ~10% higher than AERONET AODs (1020 nm). The CATS AODs are ~3% higher than CALIOP
283 AOD (1064 nm) and are ~5-10% higher than DT MODIS AODs. One possible explanation for
284 this discrepancy is because mean AODs are dominated by low AOD cases and the slopes of the
285 regression relationships are strongly affected by a few high AOD cases. Thus, it is likely that
286 CATS AODs are overestimated at the low AOD ranges and are underestimated at the high AOD
287 ranges.

288 Also note that as suggested by Omar et al., (2013), the choices of spatial and temporal
289 collocation windows have an effect on collocation results. Thus, we repeated the exercises in Figures
290 1-3 by doubling the spatial and temporal collocation windows as well as reducing the collocation
291 windows by half. The descriptive statistics of this sensitivity study are included in Table 2. While
292 the number of collocated data pairs are drastically affected by the spatial and temporal collocation
293 window sizes, less significant changes are found in descriptive statistics such as mean, median,

294 and standard deviations of AODs, as well as slopes and correlation values. The slope of DT Aqua
295 MODIS and CATS AODs, however, seems sensitive to changes in collocation methods. Changes
296 in slope of 0.61 to 0.78 are found for the change of temporal collocation window from 15 minutes
297 to 60 minutes with a fixed spatial collocation window of 0.4° Latitude/Longitude.

298 Still, larger discrepancies between CATS and CALIOP AODs during daytime indicate that
299 both sensors are susceptible to solar contamination. To overcome solar contamination and more
300 accurately detect aerosol layers, CALIOP and CATS data products are averaged up to 80 km and
301 60 km, respectively. Noel et al. (2018) found that the feature type score can be used for cloud
302 screening throughout the diurnal envelope of solar angles. To further evaluate impact of the solar
303 contamination introduced bias in the diurnal analysis in aerosol detection or products, CATS
304 AODs are evaluated as a function of local time. For each CATS observation of a given location
305 and UTC time, the associated local time is computed by adding the UTC time by 1 hour per 15°
306 Longitude away from the Prime Meridian in the east direction. Figure 4a shows the CATS AOD
307 versus local time for both global land and oceans, constructed using 6 hourly mean CATS AOD
308 binned on a 5 degree by 5 degree grid globally. While the data has additional noise, no major
309 deviations in AODs are found during either sunrise or sunset time, although we speculate that
310 larger uncertainties in CATS AODs and extinctions may be present around day and night
311 terminators. Figure 4b shows a similar plot as Figure 4a, but with the region restricted to 25° S-
312 52° S. Here, we want to investigate the variations in CATS AODs as a function of local time, over
313 relatively aerosol free oceans. We picked 25° S as the cutoff line as CATS data only available to
314 51.6° S (limited to the ISS inclination angle) and thus, this threshold is used to ensure enough data
315 samples in the analysis, although some land regions are also included. As indicated in Figure 4b,
316 again, no significant deviations in pattern are found for both sunrise and sunset time, plausibly

317 indicating that solar contamination, as speculated, may not be as significant. Comparing the mean
318 AOD at local midnight to the mean AOD at local noon by performing a student's t test, the
319 difference is not significant at the 95% confidence level, with a p-value of 0.16.

320 Figure 4c shows the difference between AERONET (1020 nm) and CATS (1064 nm) AOD
321 (Δ AOD) as a function of local time. Again, although data are rather noisy, no major pattern is
322 found near sunrise or sunset times, further indicating that solar contamination during dawn or dusk
323 times may have a less severe impact to CATS AOD retrievals from a long term mean perspective.
324 In summary, Sections 3.1.1-3.1.3 suggest that with careful QA procedures, AOD retrievals from
325 CATS are comparable to those from other existing sensors such as AERONET, MODIS, and
326 CALIOP at the same local times.

327

328 **3.1.4 CATS-CALIOP Vertical Extinction Profiles**

329 One advantage of CATS is its ability to retrieve both column-integrated AOD and vertical
330 distributions of aerosol extinction. Therefore, in this section, extinction profiles from CATS are
331 compared with that from CALIOP. Again, similar to the Section 3.1.3, collocated profiles for
332 CATS and CALIOP are first found for both retrievals that are close in space and time (within ± 30
333 minutes and 0.4 degrees latitude and longitude). However, different from Section 3.1.3, only one
334 pair of collocated CATS and CALIOP profiles, which has the closest Euclidian distance on the
335 earth's surface, is retained for each collocated incident.

336 The CATS cloud-aerosol discrimination (CAD) algorithm is a multidimensional
337 probability density function (PDF) technique that is based on the CALIPSO algorithm (Liu et al.
338 2009). The PDFs were developed based on Cloud Physics Lidar (CPL) measurements obtained
339 during over 11 field campaigns and 10 years. As shown in Figure 5e, a reasonable agreement is

340 found between CATS V3-00 aerosol extinction with CALIOP for over land. However, CATS
341 overestimates aerosol extinction around 1 km compared to CALIOP over ocean (Figure 5d). This
342 can also be seen on a plot of the difference between CATS and CALIOP 1064 nm extinction for
343 all collocated profiles, included in Figure 5f, where there is an overall positive difference around
344 1 km.

345 Due to the precessing orbit of the ISS, the CATS sampling is irregular and very different
346 compared to the sun-synchronous orbits of the A-Train sensors. These orbital differences between
347 CATS and CALIOP make comparing the data from these two sensors challenging since they are
348 fundamentally observing different locations of the Earth at different times. Thus, we shouldn't
349 expect the extinction profiles and AOD from these two sensors to completely agree. Additionally,
350 there are other algorithm and instrument differences that can lead to differences in extinction
351 coefficients and AOD. Over land where dust is the dominant aerosol type, differences in lidar
352 ratios between the two retrieval algorithms (CATS uses 40 sr while CALIOP uses 44 sr), can cause
353 CATS extinction coefficients that are up to 10% lower than CALIOP, potentially explaining the
354 higher CALIOP extinction values in Figure 5e. Over ocean, especially during daytime, differences
355 in CATS and CALIOP lidar ratios for marine and smoke aerosols can introduce a difference
356 between CATS and CALIOP extinction coefficients (Figure 5d). These difference in over ocean
357 data (Figure 5d) could also attributed to differences in CATS and CALIOP 1064 nm backscatter
358 calibration. For example, Pauly et al. (2019) reports that CATS attenuated total backscatter is
359 about 19.7% lower than PollyXT measurements in the free troposphere and 19% lower than
360 CALIOP opaque cirrus clouds due to calibration uncertainties for both sensors.

361 Also, differences in the lowest 250 m between CATS and CALIOP extinction profiles are
362 observable, which are due to how the instrument algorithms detect the surface and near-surface

363 aerosols. Both the CATS and CALIOP feature detection algorithms create a gap between the
364 surface and near-surface aerosol base altitude, despite the possible presence of aerosols in this
365 altitude region. CALIOP has an aerosol base extension algorithm that is designed to (1) detect
366 scenarios when aerosols are present in the bins just above the surface and (2) extend the near-
367 surface aerosol layer base down to the surface (Tackett et al., 2018). However, CATS does not use
368 such an algorithm so false regions of “clear-air” exist between the surface and near-surface aerosol
369 layers.

370 Vertical profiles of collocated CATS and CALIOP extinction for daytime only profiles and
371 nighttime only profiles are shown in Figure 5b and 5c, respectively. Compared to a total collocated
372 pair count of 2748 in the overall profile data, day and night profiles have 1311 and 1437 collocated
373 pairs, respectively. Again, the shapes of the CATS and the CALIOP nm extinction vertical profile
374 are similar for all three cases, despite the above mentioned offsets in altitude. Figure 5d and 5e
375 show the mean of those extinction profiles which occurred over-water and over-land, as defined
376 by the CATS surface type flag. Again in both cases CATS and CALIOP have similar shapes in
377 their vertical extinction profiles. The vertical structure of over-water extinction is also very similar
378 to that of all profiles, day, and night, which is perhaps not surprising as water profiles made up
379 2142 of 2748 (~78%) collocated pairs. The vertical structure of over-land is more different than
380 the other groups, as the extinction is higher throughout a larger depth of the atmosphere, tapering
381 off much more slowly from the surface. Furthermore, the extinction from CATS is actually lower
382 than CALIOP for over-land profiles, unlike all other categories.

383

384 **3.2 Diurnal Cycle of AODs and Aerosol Vertical Distributions**

385 Using the QAed CATS data, seasonal variations as well as diurnal variations in CATS
386 AODs are derived in this section. Diurnal variations in the vertical distributions of CATS aerosol
387 extinction are also examined at both global and regional scales.

388

389 **3.2.1 Seasonal and Diurnal Variation of AOD**

390 Figures 6a-b show the spatial distributions of CATS AODs at the 1064 nm spectral channel
391 for boreal winter-spring (Dec.-May, DJFMAM) and boreal summer-fall (June-Nov, JJASON)
392 seasons, for the period of Mar. 2015-Oct. 2017. To construct Figures 6a and 6b, quality-assured
393 CATS AODs are first binned on a 5 degree by 5 degree grid over the globe for the above mentioned
394 two bi-seasons. For each $5 \times 5^\circ$ (Latitude/Longitude) bin, for a given season, CATS AODs are
395 averaged on a pass-basis first, and then further averaged seasonally to represent AOD value of the
396 given bin. Both daytime and nighttime retrievals are included in this Figure, as well as Figures 7-
397 9.

398 In DJFMAM season, significant aerosol features are found over North Africa, Middle East,
399 India and Eastern China. For the JJASON season, besides the above mentioned regions, aerosol
400 plumes are also observable over Southern Africa, related to summer biomass burning of the region
401 (e.g. Eck et al., 2013). The seasonal-based spatial distributions of AODs from CATS, although
402 reported at the 1064 nm channel which is different from the 550 nm channel that is conventionally
403 used, are similar to some published results (e.g. Lynch et al., 2016).

404 For comparison purposes, Figures 6c-6d shows similar plots to Figures 6a-6b, but with the
405 use of CALIOP AOD at the 1064 nm spectral channel. Note that those are climatological means
406 rather than pairwise comparisons. While patterns are similar in general, at regions with peak
407 AODs of 0.4 or above for CALIOP, such as North Africa for the DJFMAM season and North

408 Africa, Middle East and India for the JJASON, much lower AODs are found for CATS. In some
409 other regions, such as over South Africa for the JJASON season, however, higher CATS AOD
410 values are observed. A table of mean AOD across each of these regions as well as over the globe
411 (within the latitude range where CATS has data) has been included for reference (Tables 3).
412 Figures 6e and 6f show the similar spatial plots as Figures 6a and 6b but with the use of Aqua
413 MODIS AODs from the DT products (using all available MODIS DT retrievals that passed QA
414 steps as described in Section 2.3). For the Aqua MODIS DT products, aerosol retrievals at the
415 short-wave Infra-red channels are only available over oceans, and thus Figures 6e-6f show only
416 over ocean retrievals. Again, while general AOD patterns look similar, discrepancies are also
417 visible, such as over the coast of south west Africa for the JJASON season and over the west coast
418 of Africa for the DJFMAM season. Those discrepancies may result from biases in each product,
419 but it is also possibly due to the differences in satellite overpass times, as CALIOP provides early
420 morning and afternoon over passes, and Aqua MODIS has an over pass time after local noon,
421 while CATS is able to report atmospheric aerosol distributions at multiple times during a day.

422 Similar to Figures 6a and 6b, Figures 7a and 7b show the spatial distribution of CATS
423 AODs, but for CATS extinction values that are below 1 km Above Ground Level (AGL) only, for
424 the DJFMAM and JJASON seasons respectively. Figure 7c and 7d show the CATS mean AOD
425 plots for extinction values from 1-2 km AGL, while Figure 7e and 7f show CATS mean AOD for
426 extinction values above 2 km AGL. For the DJFMAM season, elevated aerosol plumes with
427 altitude above 2 km AGL are found over the North Africa. For the JJASON season, elevated dust
428 plumes (> 2 km AGL) are found over North Africa and the Middle East regions, while elevated
429 smoke plumes are found over the west coast of South Africa where above cloud smoke plumes are

430 often observed during the Northern hemispheric summer season (e.g. Alfaro-Contreras et al.,
431 2016).

432 CATS has a non-sun-synchronized orbit, which enables measurements at nearly all solar
433 angles. Thus, we also constructed $5 \times 5^\circ$ (Latitude/Longitude) gridded seasonal averages (for
434 DJFMAM and JJASON seasons) of CATS AODs at 0, 6, 12 and 18 UTC that represent 4 distinct
435 times in a full diurnal cycle, as shown in Figure 8. To construct the seasonal averages, observations
436 within ± 3 hours of a given UTC time as mentioned above are averaged to represent AODs for the
437 given UTC time. On a global average, the mean AODs are 0.090, 0.089, 0.088 and 0.089 for 0, 6,
438 12 and 18 UTC respectively for the JJASON season and are 0.099, 0.096, 0.093 and 0.093 for the
439 DJFMAM season. Thus, no significant diurnal variations are found on a global scale,.

440 Still, strong diurnal variations with the maximum averaged diurnal AOD changes of above
441 0.10 can be observed for regions with significant aerosol events such as Northern Africa, Middle
442 East and India for the DJFMAM season and Northern Africa, Southern Africa, Middle East and
443 India for the JJASON season, as illustrated in Figure 9. Note that Fig. 9a shows the maximum
444 minus minimum seasonal mean AODs for the four difference times as shown in Figs. 8a,c,e,g.
445 Similarly, Fig. 9b shows the maximum minus minimum seasonal mean AODs for the four
446 difference times as shown in Figs. 8b,d,f,h. Interestingly but not unexpectedly, regions with
447 maximum diurnal variations match well with locations of heavy aerosol plumes as shown in
448 Figures 6 and 8.

449

450 **3.2.2 Diurnal variations of Aerosol Extinction on a Global Scale (both at UTC and local time)**

451 Using quality-assured CATS derived aerosol vertical distributions, mean global CATS
452 extinction vertical profiles are also generated as shown in Figure 10. Similar to steps as described

453 in the section 3.2.1, CATS extinction profiles are binned into 00, 06, 12, and 18 UTC times based
454 on the closest match in time for the JJASON and DJFMAM seasons. Figure 10a shows the daily
455 averaged CATS extinction profiles in a black line, and 00, 06, 12 and 18 UTC averaged in blue,
456 green, yellow and red lines respectively, for the DJFMAM season. Similar plot is shown in Figure
457 10d for the JJASON season. CATS extinction profiles for the daily average as well averages for
458 the four selected times are similar, suggesting that minor temporal variations in CATS extinctions
459 can be expected for global averages.

460 Those global averages are dominated by CATS profiles from global oceans (Figure 10b
461 and 10e), which also have small diurnal variations, as ~70% of the globe is covered by water. In
462 comparison, noticeable diurnal changes in aerosol vertical distributions are found over land as
463 shown in Figure 10c and 10f. For the DJFMAM season, at the 1 km altitude, the minimum and
464 maximum aerosol extinctions are at 12 and 18 UTC respectively. Similarly, the minimum and
465 maximum aerosol extinctions are at 12 and 00 UTC at the altitude of 400 m. For the JJASON
466 season, the minimum aerosol extinction values are found at 12 UTC for the whole 0-2 km column,
467 while the maximum aerosol extinction values are at 18UTC for 1.5 km and 00 UTC for the 300-
468 400 m altitude. Still, it should be noted that aerosol concentrations may be a function of local
469 time, yet for a given UTC time, local times will vary by region. Also, due to solar contamination,
470 nighttime retrievals from CATS are significantly and demonstrably less noisy than daytime retrievals,
471 and this difference in sensor sensitivity between day and night may further affect the derived
472 diurnal variations in CATS AOD and aerosol vertical profiles as shown in Figure 3 for individual
473 retrievals. Still, no apparent solar pattern is detectable from Figure 8, and only minor diurnal
474 variations are found for Figure 10a and 10d, which indicate that such a solar contamination may
475 introduce noise but not bias to daytime aerosol retrievals, from a global mean perspective.

476 If we examine the mean global CATS extinction vertical profiles with respect to local time
477 as shown in Figure 11, however, some distinct features appear. For example, Figure 11a and 11d
478 suggests that on global average, the minimum aerosol extinction below 1 km is found for 6:00 pm
479 local time, for both JJASON and DJFMAM seasons. Similar patterns are also observed for over
480 global oceans. However, for over land cases, for both seasons, the minimum and maximum aerosol
481 extinction below 600 m is found for 12:00 pm and 00:00/06:00 am local time.

482

483 **3.2.3 Diurnal variations of Aerosol Extinction on a Regional Scale (at local time)**

484 In this section, the diurnal variations of aerosol vertical distributions are studied as a
485 function of local solar time for selected regions with high mean AODs as highlighted in Figure 6.
486 We picked local solar time here as for those regional analyses. Note a near 1 to 1 transformation
487 can be achieved between UTC and local solar time. Also, as learned from the previous section,
488 aerosol features are likely to have a local time dependency. A total of four regions, including
489 Africa-North, Middle East, India and Northeast China, which show significant seasonal mean
490 AODs in Figure 6, are selected for the DJFMAM season (Figure 12). For the JJASON season
491 (Figure 13), in addition to the above mentioned 4 regions, the Africa-South region is also included
492 due to biomass burning in the region during the Northern Hemisphere summer time. The
493 Latitude/Longitude boundary of each selected region is described in Table 4. Regional-based
494 analyses are also conducted for 4 selected regions for the DJFMAM season and 5 selected regions
495 for the JJASON season at four local times: 0:00 am (midnight), 6:00 am, 12:00 pm and 6:00 pm,
496 using quality assured CATS profiles. Generally, the maximum diurnal change in aerosol
497 extinction is found at the altitude of below 1 km for all regions as well for both seasons. Also,

498 larger diurnal variations in vertical distributions of aerosol extinction are found for the JJASON
499 season, in-comparing with the DJFMAM season, while regional-based differences are apparent.

500 For the Africa-North region, dominant aerosol types are dust and smoke aerosol for the
501 DJFMAM season, and dust for the JJASON season (e.g. Remer et al., 2008). Interestingly, the
502 maximum aerosol extinction below 500m is found at 6:00 am for the DJFMAM season. While for
503 the JJASON season, the maximum aerosol extinctions are found at 0:00 am / 6:00 am for the 100-
504 500 m layer, with a significant ~10-20% higher aerosol extinction from the daily mean. Note that
505 6:00 am in the Africa-North region corresponds to early morning, which has been identified in
506 several studies (Fiedler et al., 2013; Ryder et al. 2015) as the time of day when nocturnal low-level
507 jet breakdown causes large amounts of dust emission in this region. Thus, we suspect that this
508 6:00 am peak in maximum aerosol extinctions may be the signal resulting from the low-level jet
509 ejection mechanism captured on a regional scale. As the day progresses into the afternoon and
510 early evening, we find the aerosol heights shifting upwards, likely related to the boundary layer's
511 mixed layer development.

512 For the Middle East region, for the JJASON season, a daily maximum in aerosol extinction
513 of $\sim 0.15 \text{ km}^{-1}$ is found at midnight (0:00 am) , with a daily minimum of $\sim 0.08 \text{ km}^{-1}$ found at local
514 noon (12:00 pm), for the peak aerosol extinction layer that has a daily mean aerosol extinction of
515 $\sim 0.12 \text{ km}^{-1}$. This translates to a $\sim \pm 20\text{-}30\%$ daily variation for aerosol extinction for the peak
516 aerosol extinction layer. Smaller daily variation in aerosol extinction, however, is found for the
517 same region for the DJFMAM season.

518 For the India region, for the JJASON season, a large peak in aerosol extinction of up to
519 10% higher than daily mean is found at 6:00 am below 500 m. The minimum aerosol extinction
520 is found at 12:00/6:00 pm for the layer below 500 m, and is overall $\sim 10\%$ lower than the peak

521 daily mean aerosol extinction value. For the DJFMAM season, minimum aerosol extinctions are
522 found at 12:00 pm for near the whole 0-2 km column, while for the layer below 500 m, the
523 maximum aerosol extinction values are found at mid-night (0:00 am).

524 For the Northeast China region , a significant peak found at the 500m-1km layer for local
525 afternoon (6:00 pm) for the DJFMAM season. A similar feature is also found for the JJASON
526 season. While the peak extinction for the JJASON season happens at 06:00am for the aerosol
527 layer below 500m. Lastly, for the Africa-South region, biomass burning aerosols are prevalent
528 during the summer time and thus only the JJASON season is analyzed. As shown in 13b, below
529 500m in altitude, lower extinction values are found for local afternoon (18:00 pm) and higher
530 extinction values are found for local morning or early morning (0:00 and 6:00 am).

531

532 **4.0 Conclusions**

533 Using CALIOP, MODIS and AERONET data, we evaluated CATS derived AODs as well
534 as vertical distributions of aerosol extinctions for the study period of for Mar. 2015 – Oct. 2017.
535 CATS data (at 1064 nm) were further used to study variations in AODs and aerosol vertical
536 distributions diurnally. We found:

537 (1) Quality assurance steps are critical for applying CATS data in aerosol related
538 applications. With a less than 2% data loss due to QA steps, an improvement in
539 correlation from 0.51 to 0.65 is found for the collocated CATS and AERONET AOD
540 comparisons. Using quality assured CATS data, reasonable agreements are found
541 between CATS derived AODs and AODs from CALIOP, Aqua MODIS DT and Terra
542 MODIS DT at the same local times, with correlations of 0.74, 0.74 and 0.72
543 respectively.

544 (2) While the averaged vertical distributions from CATS compare reasonably well with
545 that from CALIOP, differences in peak extinction altitudes are present. This may due
546 to sampling difference as well as algorithm and instrument differences such as different
547 lidar ratios used.

548 (3) From the global mean perspective, minor changes are found for AODs at four selected
549 times, namely 00, 06, 12 and 18 UTC. Yet noticeable diurnal variations in AODs of
550 above 0.10 (at 1064 nm) are found for regions with extensive aerosol events, such as
551 over North Africa, Middle East, and India for the DJFMAM season, and over North
552 and South of Africa, India and Middle East for the JJASON season.

553 (4) From the global mean perspective, changes are less noticeable for the averaged aerosol
554 extinction profiles at 00, 06, 12 and 18 UTC. Yet, if the study is repeated with respect
555 to local time, a peak in aerosol extinction is found for local noon (12:00pm) for the
556 DJFMAM season and the minimum value in aerosol extinction is found at 6:00 pm
557 local time for both JJASON and DJFMAM seasons. While the over water aerosol
558 vertical distributions are similar to the global means, for over land cases, the minimum
559 and maximum extinctions are found at local noon (12:00pm) and local morning or early
560 morning (6:00am and 0:00am) for the layer below 500 m for both seasons.

561 (5) Larger diurnal variations are found in regions with heavy aerosol plumes such as North
562 and South (summer season only) of Africa, Middle East, India and Eastern China. In
563 particular, aerosol extinctions from 6:00 am over North Africa are ~10% higher than
564 daily means for the 0-500 m column for both seasons. We suspect this may be related
565 to increase in dust concentrations due to breakdown of low level jets at early morning
566 time for the region.

567 (6) Still, readers should be aware that AOD retrievals at the 1064 nm are less sensitive to
568 fine mode aerosols such as smoke and pollutant aerosols, compared to coarse mode
569 aerosols such as dust aerosols (e.g. Dubovik et al., 2000). Thus, an investigation of
570 diurnal variations of aerosol properties at the visible channel may be also needed for a
571 future study.

572 This paper suggests that strong regional diurnal variations exist for both AOD and aerosol
573 extinction profiles. Still, at present these conclusions are tentative, and will remain so until a
574 comprehensive analysis of the CATS calibration accuracy and stability is completed. These results
575 demonstrate the need for global aerosol measurements throughout the entire diurnal cycle to
576 improve visibility and particulate matter forecasts as well as studies focused on aerosol climate
577 applications.

578

579 **Author Contribution:**

580 Authors J. Zhang, J. S. Reid and L. Lee designed the study. L. Lee worked on data processing for
581 the project. J. E. Yorks guided L. Lee on data processing. The manuscript was written with inputs
582 from all coauthors.

583 **Acknowledgments:**

584 We acknowledge the support of ONR grant (N00014-16-1-2040) and NASA grant
585 (NNX17AG52G) for this study. L. Lee is also partially supported by the NASA NESSF
586 fellowship grant (NNX16A066H). J. S Reid's participation was supported by the Office of Naval
587 Research Code 322 and 33. We thank the NASA AERONET team for the AERONET data used
588 in this study. CATS and CALIOP data were obtained from the NASA Langley Research Center

589 Atmospheric Science Data Center. MODIS aerosol products were obtained from the NASA
590 Goddard Space Flight Center's MODIS Adaptive Processing System (MODAPS) site. We thank
591 Mark Vaughan and other two anonymous reviewers for their constructive suggestions and
592 comments.
593

594 **References:**

- 595 Aerosol Product Application Team of the AWG Aerosols/Air Quality/Atmospheric Chemistry
596 Team: GOES-R Advanced Baseline Imager (ABI) algorithm theoretical basis document
597 for suspended matter/aerosol optical depth and aerosol size parameter,
598 NOAA/NESDIS/STAR July 2012,
599 <https://www.star.nesdis.noaa.gov/goesr/docs/ATBD/AOD.pdf> (last accessed on Nov. 17,
600 2018).
- 601 Alfaro-Contreras, R., Zhang, J., Campbell, J. R., and Reid, J. S.: Investigating the frequency
602 and trends in global above-cloud aerosol characteristics with CALIOP and OMI, *Atmos.*
603 *Chem. Phys.*, 16, 47-69, doi:10.5194/acp-16-47-2016, 2016.
- 604 Campbell, J. R., Tackett, J. L., Reid, J. S., Zhang, J., Curtis, C. A., Hyer, E. J., Sessions, W.
605 R., Westphal, D. L., Prospero, J. M., Welton, E. J., Omar, A. H., Vaughan, M. A., and
606 Winker, D. M.: Evaluating nighttime CALIOP 0.532 μm aerosol optical depth and
607 extinction coefficient retrievals, *Atmos. Meas. Tech.*, 5, 2143-2160,
608 <https://doi.org/10.5194/amt-5-2143-2012>, 2012.
- 609 CATS Algorithm Theoretical Basis Document:
610 https://cats.gsfc.nasa.gov/media/docs/CATS_ATBD_V1-02.pdf, 2016; accessed on March
611 28, 2019.
- 612 Christopher, S. A. and Zhang, J.: Daytime variation of shortwave direct radiative forcing of
613 biomass burning aerosols from GOES 8 imager, *J. Atmos. Sci.*, 59, 681–691, 2002.
- 614 Dubovik, O., Smirnov, A., Holben, B. N., King, M. D., Kaufman, Y. J., Eck, T. F., and
615 Slutsker, I.: Accuracy Assessments of Aerosol Optical Properties Retrieved from Aerosol

616 Robotic Network (AERONET) Sun and Sky Radiance Measurements, *J. Geophys. Res.-*
617 *Atmos.*, 105, 9791–9806, <https://doi.org/10.1029/2000JD900040>, 2000.

618 Eck, T .F., Holben, B. N., Reid, J. S., Mukelabai, M. M., Piketh, S. J., Torres, O., Jethva, H.
619 T., Hyer, E. J., Ward, D. E., Dubovik, O., and Sinyuk, A.: A seasonal trend of single
620 scattering albedo in southern African biomass-burning particles: Implications for satellite
621 products and estimates of emissions for the world’s largest biomass-burning source, *J.*
622 *Geophys. Res.-Atmos.*, 118, 6414–6432, 2013.

623 Fiedler, S., Schepanski, K., Heinold, B., Knippertz, P., and Tegen, I.: Climatology of
624 nocturnal low-level jets over North Africa and implications for modeling mineral dust
625 emission, *J. Geophys. Res. Atmos.*, 118, 6100–6121, doi: 10.1002/jgrd.50394, 2013.

626 Giglio, L., Kendall, J.D., Mack, R.: A multi-year active fire dataset for the tropics derived from
627 the TRMM VIRS., *International Journal of Remote Sensing* 24, 4505-4525, 2003.

628 Giles, D. M., Sinyuk, A., Sorokin, M. G., Schafer, J. S., Smirnov, A., Slutsker, I., Eck, T. F.,
629 Holben, B. N., Lewis, J. R., Campbell, J. R., Welton, E. J., Korkin, S. V., and Lyapustin,
630 A. I.: Advancements in the Aerosol Robotic Network (AERONET) Version 3 database –
631 automated near-real-time quality control algorithm with improved cloud screening for Sun
632 photometer aerosol optical depth (AOD) measurements, *Atmos. Meas. Tech.*, 12, 169-209,
633 <https://doi.org/10.5194/amt-12-169-2019>, 2019.

634 Heinold, B., Knippertz, P., Marsham, J. H., Fiedler, S., Dixon, N. S., Schepanski, K., Laurent,
635 B., and Tegen, I.: The role of deep convection and nocturnal low-level jets for dust
636 emission in summertime West Africa: Estimates from convection-permitting
637 simulations, *J. Geophys. Res. Atmos.*, 118, 4385–4400, doi:10.1002/jgrd.50402, 2013.

638 Holben, B. N., and coauthors: AERONET—A Federated Instrument Network and Data
639 Archive for Aerosol Characterization. *Remote Sensing of Environment*, 66(1), 1–16.
640 [https://doi.org/10.1016/S0034-4257\(98\)00031-5](https://doi.org/10.1016/S0034-4257(98)00031-5), 1998.

641 Hyer, E. J., Reid, J. S., Prins, E. M., Hoffman, J. P., Schmidt, C. C., Miettinen, J. I., and Giglio,
642 L.: Different views of fire activity over Indonesia and Malaysia from polar and
643 geostationary satellite observations, *Atmos. Res.*, 122, 504-519, 2013.

644 Kaku K. C., Reid, J. S., Hand, J. L., Edgerton, E. S., Holben, B. N., Zhang, J., and Holz, R. E.:
645 Assessing the challenges of surface-level aerosol mass estimates from remote sensing
646 during the SEAC4RS campaign: Baseline surface observations and remote sensing in the
647 Southeastern United States, *JGR*, doi: 10.1029/2017JD028074, 2018.

648 Levy, R. C., Mattoo, S., Munchak, L. A., Remer, L. A., Sayer, A. M., Patadia, F., and Hsu, N.
649 C.: The Collection 6 MODIS aerosol products over land and ocean. *Atmos. Meas. Tech.*,
650 6(11), 2989–3034. <https://doi.org/10.5194/amt-6-2989-2013>, 2013.

651 Liu, Z., and coauthors: The CALIPSO Lidar Cloud and Aerosol Discrimination: Version 2
652 Algorithm and Initial Assessment of Performance, *J. Atmos. Oceanic Technol.*, 26, 1198–
653 1213, 2009.

654 Lynch, P., Reid, J. S., Westphal, D. L., Zhang, J., Hogan, T. F., Hyer, E. J., Curtis, C. A., Hegg,
655 D. A., Shi, Y., Campbell, J. R., Rubin, J. I., Sessions, W. R., Turk, F. J., and Walker, A.
656 L.: An 11-year global gridded aerosol optical thickness reanalysis (v1.0) for atmospheric
657 and climate sciences, *Geosci. Model Dev.*, 9, 1489-1522, [https://doi.org/10.5194/gmd-9-](https://doi.org/10.5194/gmd-9-1489-2016)
658 1489-2016, 2016.

659 Mbourou, G. N., Berand, J. J., and Nicholson, S. E.: The diurnal and seasonal cycle of wind-
660 borne dust over Africa north of the equator, *J. Appl. Meteor.*, 36, 868-882, 1997.

661 McGill, M. J., Yorks, J. E., Scott, V. S., Kupchock, A. W., and Selmer, P. A.: The Cloud-
662 Aerosol Transport System (CATS): A technology demonstration on the International Space
663 Station, Proc. SPIE 9612, Lidar Remote Sensing for Environmental Monitoring XV,
664 96120A, doi:10.1117/12.2190841, 2015.

665 Noel, V., Chepfer, H., Chiriaco, M., and Yorks J. E.: The diurnal cycle of cloud profiles over
666 land and ocean between 51° S and 51° N, seen by the CATS spaceborne lidar from the
667 International Space Station, Atmos. Chem. Phys., 18, 9457-9473,
668 <https://doi.org/10.5194/acp-18-9457-2018>, 2018.

669 Omar, A. H., Winker, D. M., Tackett, J. L., Giles, D. M., Kar, J., Liu, Z., Vaughan, M. A.,
670 Powell, K. A., and Trepte C. R.: CALIOP and AERONET aerosol optical depth
671 comparisons: One size fits none, J. Geophys. Res. Atmos., 118, 4748–4766, doi:
672 10.1002/jgrd.50330, 2013.

673 Pauly, R. M., Yorks, J. E., Hlavka, D. L., McGill, M. J., Amiridis, V., Palm, S. P., Rodier, S.
674 D., Vaughan, M. A., Selmer, P. A., Kupchock, A. W., Baars, H., and Gialitaki, A.: Cloud
675 Aerosol Transport System (CATS) 1064 nm Calibration and Validation, Atmos. Meas.
676 Tech. Discuss., <https://doi.org/10.5194/amt-2019-172>, in review, 2019.

677 Rajapakshe, C., Zhang, Z., Yorks, J. E., Yu, H., Tan, Q., Meyer, K., Platnick, S.: Seasonally
678 Transported Aerosol Layers over Southeast Atlantic are Closer to Underlying Clouds than
679 Previously Reported, Geophys. Res. Lett., 44, doi:10.1002/2017GL073559, 2017.

680 Redemann, J., Vaughan, M. A., Zhang, Q., Shinozuka, Y., Russell, P. B., Livingston, J. M., ...
681 Remer, L. A.: The comparison of MODIS-Aqua (C5) and CALIOP (V2 & V3) aerosol
682 optical depth. Atmospheric Chemistry and Physics, 12(6), 3025–3043.
683 <https://doi.org/https://doi.org/10.5194/acp-12-3025-2012>, 2012.

684 Reid, J.S., Eck, T. F., Christopher, S. A., Hobbs, P. V., and Holben B. R.: Use of the Angstrom
685 exponent to estimate the variability of optical and physical properties of aging smoke
686 particles in Brazil, *J. Geophys. Res.*, *104*, 27,489-27,489, 1999.

687 Remer, L. A., and coauthors: Global aerosol climatology from the MODIS satellite sensors, *J.*
688 *Geophys. Res.*, *113*, D14S07, doi: 10.1029/2007JD009661, 2008.

689 Remer, L.A., Y.J. Kaufman, D. Tanré, S. Mattoo, D.A. Chu, J.V. Martins, R. Li, C. Ichoku,
690 R.C. Levy, R.G. Kleidman, T.F. Eck, E. Vermote, and B.N. Holben, [The MODIS Aerosol](#)
691 [Algorithm, Products, and Validation](#). *J. Atmos. Sci.*, **62**, 947–973,
692 <https://doi.org/10.1175/JAS3385.1>, 2005.

693 Ryder, C. L., McQuaid, J. B., Flamant, C., Rosenberg, P. D., Washington, R., Brindley, H. E.,
694 Highwood, E. J., Marsham, J. H., Parker, D. J., Todd, M. C., Banks, J. R., Brooke, J. K.,
695 Engelstaedter, S., Estelles, V., Formenti, P., Garcia-Carreras, L., Kocha, C., Marengo, F.,
696 Sodemann, H., Allen, C. J. T., Bourdon, A., Bart, M., Cavazos-Guerra, C., Chevaillier, S.,
697 Crosier, J., Darbyshire, E., Dean, A. R., Dorsey, J. R., Kent, J., O'Sullivan, D., Schepanski,
698 K., Szpek, K., Trembath, J., and Woolley, A.: Advances in understanding mineral dust and
699 boundary layer processes over the Sahara from Fennec aircraft observations, *Atmos. Chem.*
700 *Phys.*, *15*, 8479-8520, <https://doi.org/10.5194/acp-15-8479-2015>, 2015.

701 Shi Y., Zhang, J., Reid, J. S., Hyer, E., and Hsu, N. C.: Critical evaluation of the MODIS Deep
702 Blue aerosol optical depth product for data assimilation over North Africa, *Atmos. Meas.*
703 *Tech.*, *6*, 949-969, doi:10.5194/amt-6-949-2013, 2013.

704 Shi Y., Zhang J., Reid J. S., Hyer E. J., Eck T. F., and Holben B. N.: A critical examination of
705 spatial biases between MODIS and MISR aerosol products – application for potential
706 AERONET deployment, *Atmos. Meas. Tech.*, *4*, 2823–2836, 2011.

707 Stephens, G. L., and coauthors: The CLOUDSAT mission and the A-TRAIN, Bulletin of the
708 American Meteorological Society, 83(12), 1771–1790. [https://doi.org/10.1175/BAMS-83-](https://doi.org/10.1175/BAMS-83-12-1771)
709 [12-1771](https://doi.org/10.1175/BAMS-83-12-1771), 2002.

710 Tackett, J. L., Winker, D. M., Getzewich, B. J., Vaughan, M. A., Young, S. A., and Kar, J.:
711 CALIPSO lidar level 3 aerosol profile product: version 3 algorithm design, Atmos. Meas.
712 Tech., 11, 4129-4152, <https://doi.org/10.5194/amt-11-4129-2018>, 2018.

713 Tiwari, S., Srivastava, A. K., Bisht, D. S., Parmita, P., Srivastava, M. K., and Atri, S. D.:
714 Diurnal and seasonal variations of black carbon and PM2.5 over New Delhi, India:
715 Influence of meteorology, Atmos. Res, 125, 50-62, doi:10.1016/j.atmos.res.2013.01.011,
716 2013.

717 Toth, T. D., Campbell, J. R., Reid, J. S., Tackett, J. L., Vaughan, M. A., Zhang, J., & Marquis,
718 J. W.: Minimum aerosol layer detection sensitivities and their subsequent impacts on
719 aerosol optical thickness retrievals in CALIPSO level 2 data products. Atmospheric
720 Measurement Techniques, 11(1), 499–514. [https://doi.org/https://doi.org/10.5194/amt-11-](https://doi.org/https://doi.org/10.5194/amt-11-499-2018)
721 [499-2018](https://doi.org/https://doi.org/10.5194/amt-11-499-2018), 2018.

722 Toth, T. D., Zhang, J., Campbell, J. R., Reid, J. S., & Vaughan, M. A.: Temporal variability of
723 aerosol optical thickness vertical distribution observed from CALIOP, Journal of
724 Geophysical Research: Atmospheres, 121(15), 9117–9139.
725 <https://doi.org/10.1002/2015JD024668>, 2016.

726 Vaughan, M., Garnier, A., Josset, D., Avery, M., Lee, K.-P., Liu, Z., Hunt, W., Pelon, J., Hu,
727 Y., Burton, S., Hair, J., Tackett, J. L., Getzewich, B., Kar, J., and Rodier, S.: CALIPSO
728 lidar calibration at 1064 nm: version 4 algorithm, Atmos. Meas. Tech., 12, 51-82,
729 <https://doi.org/10.5194/amt-12-51-2019>, 2019.

730 Wang, J., Liu, X., Christopher, S. A., Reid, J. S., Reid, E. A., and Maring, H.: The effects of
731 non-sphericity on geostationary satellite retrievals of dust aerosols, *Geophys. Res. Lett.*,
732 30(24), 2293, doi:10.1029/2003GL018697, 2003.

733 Winker, D. M., and coauthors: Overview of the CALIPSO Mission and CALIOP Data
734 Processing Algorithms. *Journal of Atmospheric and Oceanic Technology*, 26(11), 2310–
735 2323. <https://doi.org/10.1175/2009JTECHA1281.1>, 2009.

736 Young, S. A., M. A. Vaughan, R. E. Kuehn, and D. M. Winker, 2013: The Retrieval of Profiles
737 of Particulate Extinction from Cloud-Aerosol Lidar Infrared Pathfinder Satellite
738 Observations (CALIPSO) Data: Uncertainty and Error Sensitivity Analyses, *J. Atmos.*
739 *Oceanic Technol.*, 30, 395-428, doi:10.1175/JTECH-D-12-00046.1.

740 Yorks, J. E., P.A. Selmer, E.P. Nowottnick, S.D. Rodier, M.A. Vaughan, N. Dacic, M.J.
741 McGill, and S.P. Palm, CATS Level 2 Vertical Feature Mask Algorithms and Data
742 Products: An Overview and Initial Assessment, *Atmos. Meas. Tech. Discuss.*, in
743 preparation, 2019.

744 Yorks, J. E., McGill, M. J., Palm, S. P., Hlavka, D. L., Selmer, P. A., Nowottnick, E., Vaughan,
745 M. A., Rodier, S., and Hart W. D.: An Overview of the CATS Level 1 Data Products and
746 Processing Algorithms, *Geophys. Res. Lett.*, 43, doi:[10.1002/2016GL068006](https://doi.org/10.1002/2016GL068006), 2016.

747 Yoshida M., Kikuchi, M., Nagao, T. M., Murakami, H., Nomaki, T., and Higurashi, A.:
748 Common Retrieval of Aerosol Properties for Imaging Satellite Sensors, *Journal of the*
749 *Meteorological Society of Japan*. Ser. II, Article ID 2018-039, [Advance publication],
750 <https://doi.org/10.2151/jmsj.2018-039>, 2018.

751 Zhao, X. J., Zhang, X. L., Xu, X. F., Xu, J., Meng, W., and Pu, WW.: Seasonal and diurnal
752 variation of ambient PM_{2.5} concentrations in urban and rural environments in Beijing,
753 Atmos. Environ., 43, 2893-2900, doi: 10.106/j.atmosenv.2009.03.009., 2009.
754

755 Table 1. Descriptive statistical properties between collocated CATS and AERONET, CALIOP and Aqua MODIS AOD retrievals.
 756 Here STDDEV indicates standard deviation of AOD and R-value represents the correlation coefficient.

Sensor	No. of Points	Slope	R-value	Mean AOD	Median AOD	Max AOD	Min AOD	STDDEV	CATS Mean AOD	CATS Median AOD	CATS Max AOD	CATS Min AOD	CATS STDDEV
AERONET	2240	0.56	0.65	0.088	0.054	0.98	0.001	0.103	0.099	0.058	1.31	0.0004	0.119
MODIS Aqua	3529	0.7	0.74	0.067	0.048	0.81	0.0004	0.07	0.07	0.053	1.76	0.002	0.075
MODIS Terra	2334	0.74	0.72	0.076	0.056	0.9	0.0013	0.081	0.084	0.065	1.13	0.0063	0.079
CALIOP	2762	0.74	0.74	0.089	0.063	1.01	0	0.102	0.092	0.065	1.1	0.0018	0.1

757
 758
 759
 760
 761
 762
 763
 764
 765
 766
 767
 768
 769
 770
 771
 772
 773

774 Table 2. Sensitivity study of descriptive statistical properties between collocated CATS and AERONET, CALIOP and Aqua MODIS
 775 AOD retrievals by varying spatial and temporal collocation windows. Here STDDEV indicates standard deviation of AOD and R-
 776 value represents the correlation coefficient.
 777

Collocation Thresholds	AERONET/CATS			AERONET					CATS				
	No. of Points	Slope	R-value	Mean AOD	Median AOD	Max AOD	Min AOD	STDDEV	Mean AOD	Median AOD	Max AOD	Min AOD	STDDEV
<i>Spatial (30 min.)</i>													
0.2°	904	0.54	0.63	0.092	0.052	0.82	0.002	0.107	0.102	0.058	1.31	0.0004	0.124
0.4°	2240	0.56	0.65	0.088	0.054	0.98	0.001	0.103	0.099	0.058	1.31	0.0004	0.119
0.8°	5114	0.53	0.63	0.087	0.052	0.98	0.001	0.105	0.097	0.055	2	0.0004	0.125
<i>Temporal (0.4° lat./lon.)</i>													
15 minutes	1931	0.54	0.63	0.089	0.053	0.98	0.001	0.105	0.1	0.057	1.34	0.0004	0.123
30 minutes	2240	0.56	0.65	0.088	0.054	0.98	0.001	0.103	0.099	0.058	1.31	0.0004	0.119
60 minutes	2695	0.55	0.64	0.087	0.053	0.98	0.001	0.103	0.098	0.057	1.32	0.0004	0.118
Collocation Thresholds	CALIOP/CATS			CALIOP					CATS				
<i>Spatial (30 min.)</i>													
0.2°	1948	0.73	0.76	0.088	0.063	1.15	0	0.104	0.092	0.065	1.12	0.0013	0.1
0.4°	2762	0.74	0.74	0.089	0.063	1.01	0	0.102	0.092	0.065	1.1	0.0018	0.1
0.8°	5070	0.80	0.74	0.089	0.063	0.94	0	0.099	0.093	0.066	1.61	0.0008	0.107
<i>Temporal (0.4° lat./lon.)</i>													
15 minutes	1392	0.76	0.77	0.09	0.063	0.95	0	0.104	0.092	0.066	1.1	0.0024	0.102
30 minutes	2762	0.74	0.74	0.089	0.063	1.01	0	0.102	0.092	0.065	1.1	0.0018	0.1
60 minutes	5602	0.74	0.75	0.09	0.063	1.4	0	0.104	0.093	0.066	1.55	0.0007	0.103
Collocation Thresholds	MODIS Aqua/CATS			MODIS Aqua					CATS				
<i>Spatial (30 min.)</i>													
0.2°	2998	0.73	0.75	0.062	0.043	0.86	0.0004	0.073	0.07	0.052	1.74	0.003	0.075
0.4°	3529	0.7	0.74	0.067	0.048	0.81	0.0004	0.07	0.07	0.053	1.76	0.002	0.075
0.8°	4107	0.67	0.74	0.07	0.053	0.79	0.0004	0.066	0.071	0.053	1.71	0.003	0.073
<i>Temporal (0.4° lat./lon.)</i>													
15 minutes	1814	0.61	0.71	0.064	0.048	0.82	0.0004	0.067	0.069	0.052	1.76	0.003	0.078
30 minutes	3529	0.70	0.74	0.067	0.048	0.81	0.0004	0.07	0.07	0.053	1.76	0.002	0.075
60 minutes	6490	0.78	0.76	0.069	0.049	1.21	0.0004	0.076	0.072	0.054	1.76	0.003	0.074

778
779

780 Table 3. CALIOP and CATS mean AODs / AOD standard deviations for regions as highlighted in Figure 6 and globally between +/-
 781 52° latitude.

782

Region	Latitude	Longitude	Mean CATS AOD (DJFMAM/JJASON)	Mean CALIOP AOD (DJFMAM/JJASON)	Mean CATS Standard Deviation (DJFMAM/JJASON)	Mean CALIOP Standard Deviation (DJFMAM/JJASON)
Global	52°S-52°N	180°W-180°E	0.09/0.10	0.09/0.09	0.037/0.039	0.036/0.034
India	7.5°N - 32.5°N	65°E - 85°E	0.22/0.26	0.22 /0.28	0.068/0.072	0.072/0.078
Africa - North	2.5°N - 22.5°N	35°W - 20°E	0.25/0.24	0.30 /0.25	0.062/0.064	0.075/0.067
Africa - South	17.5°S - 2.5°N	0° - 30°E	0.12/0.20	0.15 /0.13	0.037/0.048	0.038/0.038
Middle East	12.5°N - 27.5°N	35°E - 50°E	0.23/0.35	0.26/0.35	0.076/0.099	0.082/0.091
China	27.5°N - 37.5°N	110°E - 120°E	0.20/0.17	0.21 /0.16	0.061/0.056	0.074/0.060

783

784

785 Table 4. Geographic ranges, height above ground level of maximum extinction, diurnal extinction range at height of maximum
 786 extinction, and time (local) of peak extinction for the boxed red regions in Figure 6 and vertical profiles shown in Figures 12 and 13.

DJFMAM/JJASON					
Region	Latitude	Longitude	Height AGL (m) of Max. Extinction	Extinction Range (km^{-1}) at Height AGL of Max. Extinction	Time of Peak Extinction at Height AGL of Max. Extinction
India	7.5°N - 32.5°N	65°E - 85°E	180/360	0.099-0.136/0.135-0.163	0 am/6 am
Africa - North	2.5°N - 22.5°N	35°W - 20°E	420/420	0.107-0.121/0.082-0.113	6 am/6 am
Africa - South	17.5°S - 2.5°N	0° - 30°E	/420	/0.092-0.126	/6 am
Middle East	12.5°N - 27.5°N	35°E - 50°E	180/240	0.075-0.121/0.086-0.156	0 am/0 am
China	27.5°N - 37.5°N	110°E - 120°E	180/240	0.098-0.148/0.086-0.132	6 am/6 am

787
788

789 **Figure Captions**

790

791 **Figure 1.** Collocated AERONET 1020 nm AOT vs. CATS 1064 nm AOD a) without CATS QA
792 applied, and b) with CATS QA applied.

793 **Figure 2.** Collocated MODIS C6.1 a) Terra and b) Aqua interpolated 1064 nm AOD vs. CATS
794 1064 nm AOD with CATS QA applied.

795 **Figure 3.** Collocated CALIOP 1064 nm AOD vs. CATS 1064 nm AOD with CATS QA applied
796 for a) both day and night, b) nighttime over-land, c) nighttime over-water, d) daytime over-land,
797 e) daytime over-water.

798 **Figure 4:** CATS 1064 nm AOD a) as a function of local time for the globe, and b) as a function
799 of local time for areas south of -25 degrees. The difference between CATS 1064 nm AOD and
800 AERONET 1020 nm AOD as a function of local time is shown in c). The mean is represented
801 by the blue line, while the median is the green line.

802 **Figure 5.** CATS and CALIOP vertical profiles of 1064 nm extinction for a) all profiles, b)
803 daytime only, c) nighttime only, d) over-water, and e) over land. f) shows the difference between
804 CATS and CALIOP mean 1064 nm extinction for all collocated profiles (5a) as a function of
805 height. Mean AOD values are as follows: for CATS: a) 0.094 , b) 0.091 , c) 0.098, d) 0.088, e)
806 0.119, and for CALIOP: a) 0.093, b) 0.092, c) 0.093, d) 0.084, e) 0.127.

807 **Figure 6.** Mean AOD (1064 nm) by season for a) DJFMAM CATS, b) JJASON CATS, c)
808 DJFMAM CALIOP, d) JJASON CALIOP, e) DJFMAM MODIS Aqua, and f) JJASON MODIS
809 Aqua. Red boxes indicate locations of regional vertical distributions in Figures 12 and 13.

810 **Figure 7.** Mean CATS AOD (1064 nm) by season for a) DJFMAM below 1 km AGL, b)
811 JJASON below 1 km AGL, c) DJFMAM 1-2 km AGL, d) JJASON 1-2 km AGL, e) DJFMAM
812 above 2 km AGL, and f) JJASON above 2 km AGL.

813 **Figure 8.** Seasonal Mean AOD (1064 nm) binned by every 6-hours for a) DJFMAM 0 UTC, b)
814 JJASON 0 UTC, c) DJFMAM 6 UTC, d) JJASON 6 UTC, e) DJFMAM 12 UTC, f) JJASON 12
815 UTC, g) DJFMAM 18 UTC, and h) JJASON 18 UTC.

816 **Figure 9.** Maximum minus minimum mean seasonal AOD (1064 nm) for a) DJFMAM, and b)
817 JJASON.

818 **Figure 10.** Global mean 6-hourly vertical profiles of CATS 1064 nm extinction for a) DJFMAM
819 all profiles, b) DJFMAM water profiles, c) DJFMAM not-water profiles, d) JJASON all profiles,
820 e) JJASON water profiles, f) JJASON not-water profiles. Mean AODs are as follows: a) 0.084,
821 b) 0.078, c) 0.098, d) 0.089, e) 0.082, and f) 0.102.

822 **Figure 11.** Global mean 6-hourly local time (0:00 am, 6:00 am, 12:00 pm and 6:00 pm) vertical
823 profiles of CATS 1064 nm extinction for a) DJFMAM all profiles, b) DJFMAM water profiles, c)
824 DJFMAM not-water profiles, d) JJASON all profiles, e) JJASON water profiles, f) JJASON not-
825 water profiles. Mean AODs are as follows: a) 0.080, b) 0.079, c) 0.095, d) 0.082, e) 0.081, and f)
826 0.105.

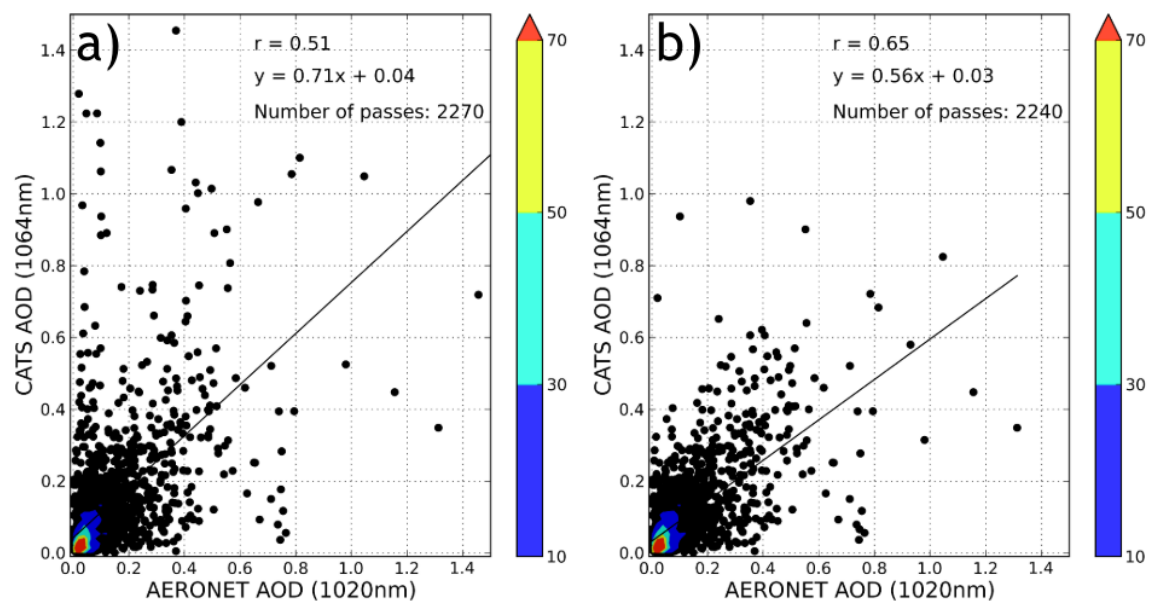
827

828 **Figure 12.** DJFMAM 6-hourly average (local time; 0:00 am, 6:00 am, 12:00 pm and 6:00 pm)
829 vertical profiles of CATS 1064 nm for locations shown in Figure 6a; a) Africa-North, b) Middle
830 East, c) India, and d) Northeast China.

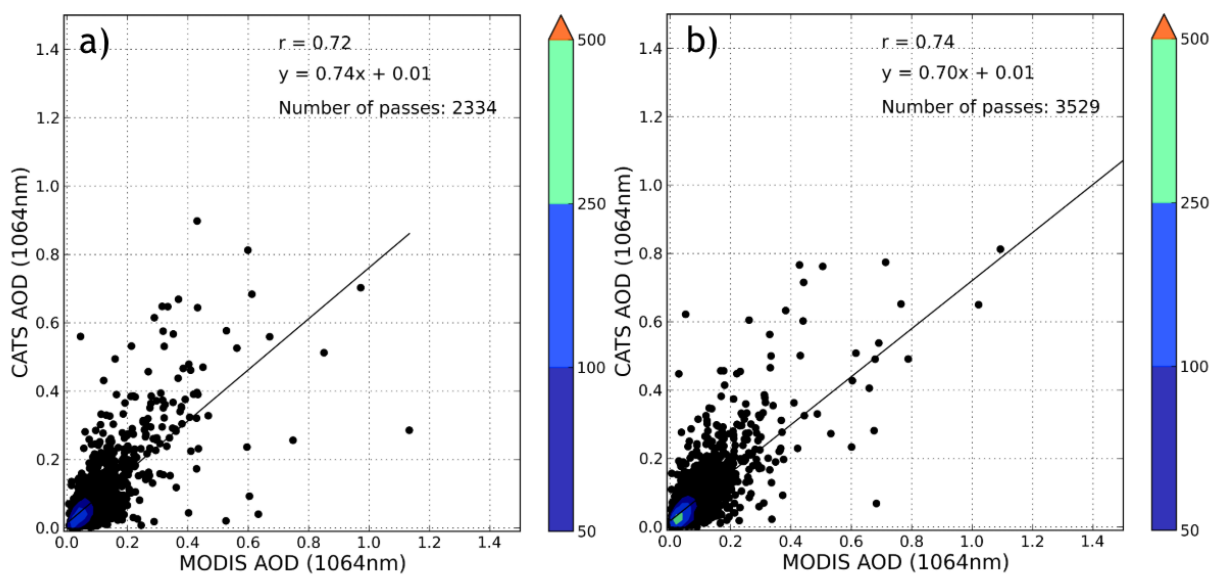
831

832 **Figure 13.** JJASON 6-hourly average (local time; 0:00 am, 6:00 am, 12:00 pm and 6:00 pm)
833 vertical profiles of CATS 1064 nm for locations shown in Figure 6b; a) Africa-North, b) Africa-
834 South, c) Middle East, d) India, and e) Northeast China.

835

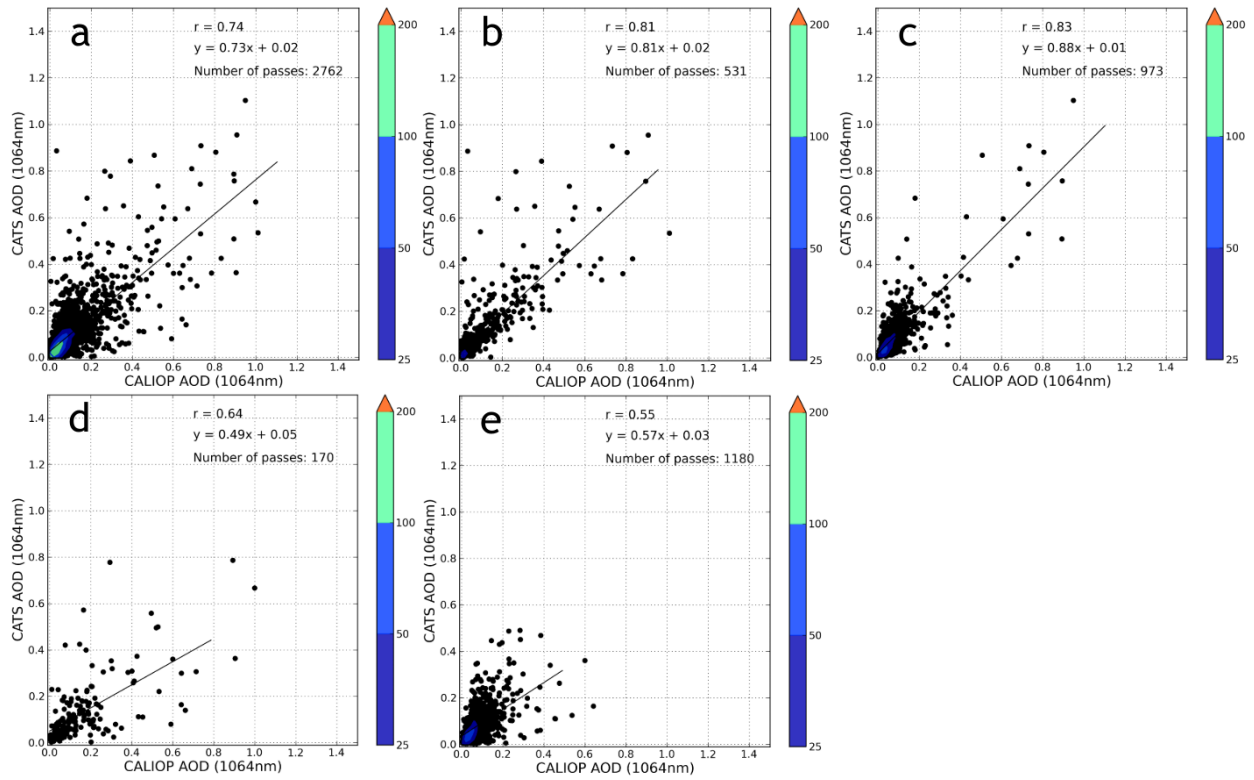


836
 Figure 1. Collocated AERONET 1020 nm AOT vs. CATS 1064 nm AOD a) without CATS QA applied, and b) with CATS QA applied.



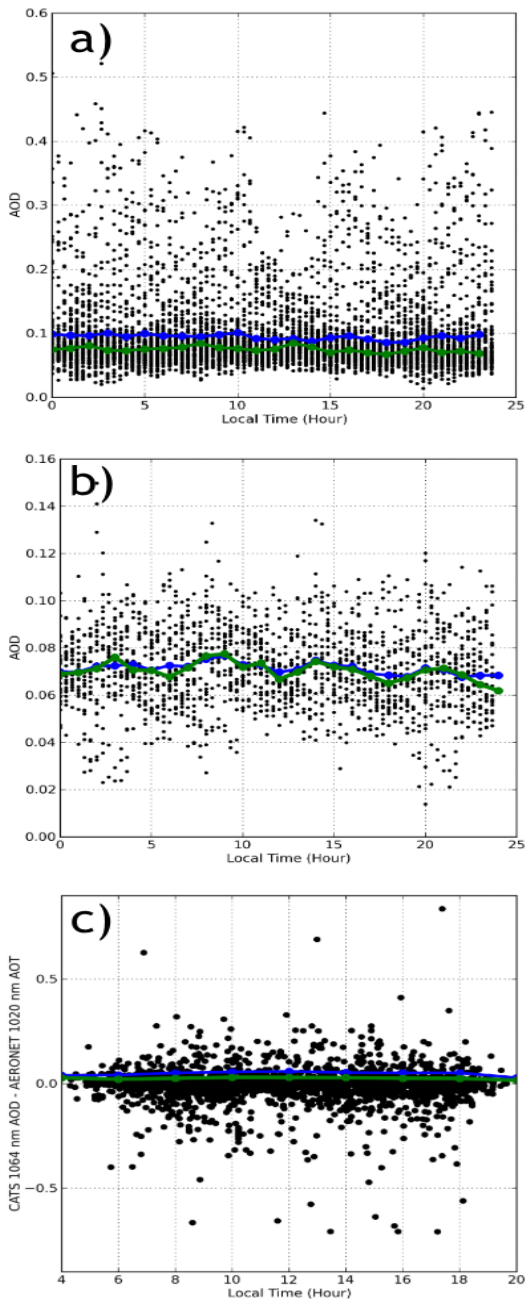
837

Figure 2. Collocated MODIS C6.1 a) Terra and b) Aqua interpolated 1064 nm AOD vs. CATS 1064 nm AOD with CATS QA applied.



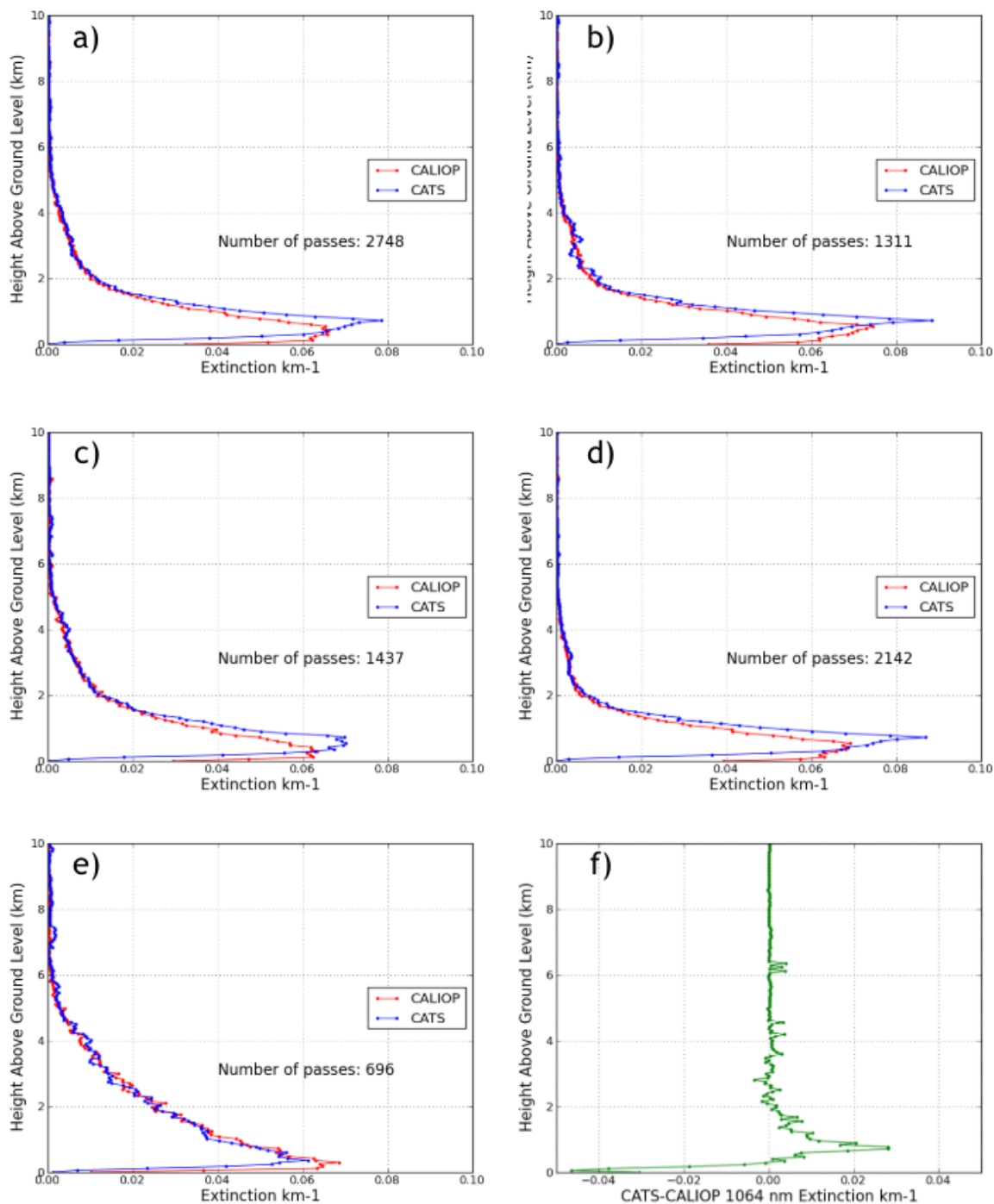
838

Figure 3. Collocated CALIOP 1064 nm AOD vs. CATS 1064 nm AOD with CATS QA applied for a) both day and night, b) nighttime over-land, c) nighttime over-water, d) daytime over-land, e) daytime over-water.



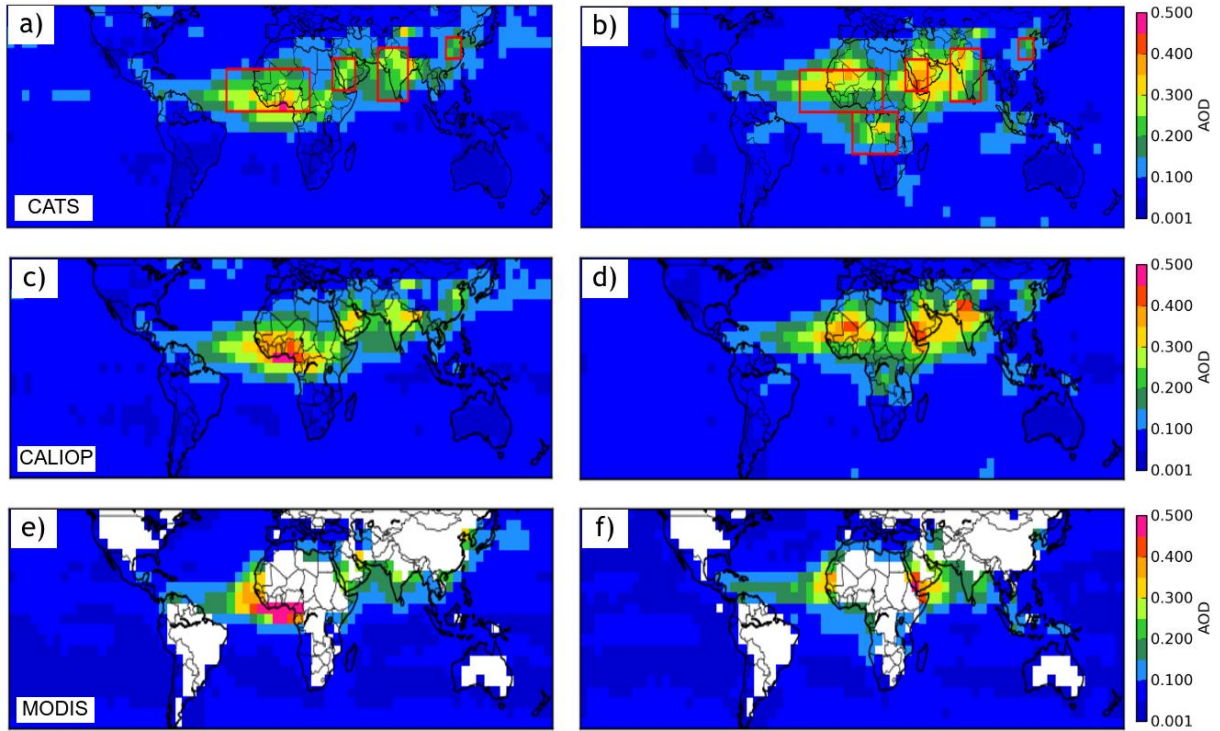
839

Figure 4. CATS 1064 nm AOD a) as a function of local time for the globe, and b) as a function of local time for areas south of -25 degrees. The difference between CATS 1064 nm AOD and AERONET 1020 nm AOD as a function of local time is shown in c). The mean is represented by the blue line, while the median is the green line.



840

Figure 5. CATS and CALIOP vertical profiles of 1064 nm extinction for a) all profiles, b) daytime only, c) nighttime only, d) over-water, and e) over land. f) shows the difference between CATS and CALIOP mean 1064 nm extinction for all collocated profiles (5a) as a function of height. Mean AOD values are as follows: for CATS: a) 0.094 , b) 0.091 , c) 0.098, d) 0.088, e) 0.119, and for CALIOP: a) 0.093, b) 0.092, c) 0.093, d) 0.084, e) 0.127.



841

842

Figure 6. Mean AOD (1064 nm) by season for a) DJFMAM CATS, b) JJASON CATS, c) DJFMAM CALIOP, d) JJASON CALIOP, e) DJFMAM MODIS Aqua, and f) JJASON MODIS Aqua. Red boxes indicate locations of regional vertical distributions in Figures 12 and 13.

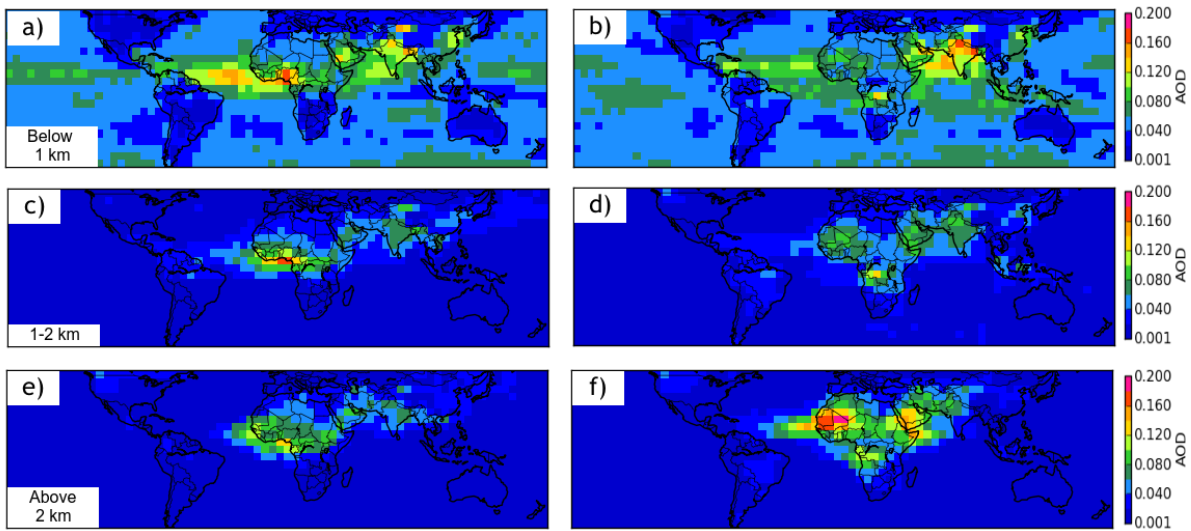
843

844

845

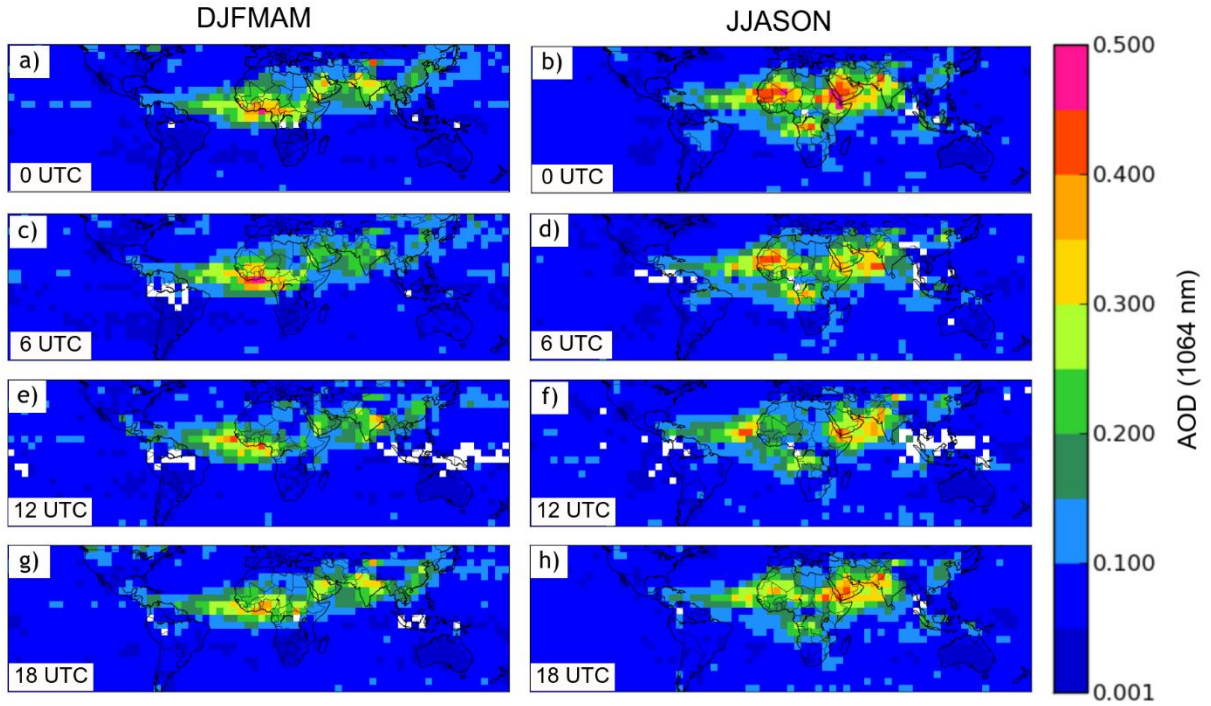
846

847



848

Figure 7. Mean CATS AOD (1064 nm) by season for a) DJFMAM below 1km AGL, b) JJASON below 1 km AGL, c) DJFMAM 1-2 km AGL, d) JJASON 1-2 km AGL, e) DJFMAM above 2 km AGL, and f) JJASON above 2 km AGL.



849

Figure 8. Seasonal Mean AOD (1064 nm) binned by every 6-hours for a) DJFMAM 0 UTC, b) JJASON 0 UTC, c) DJFMAM 6 UTC, d) JJASON 6 UTC, e) DJFMAM 12 UTC, f) JJASON 12 UTC, g) DJFMAM 18 UTC, and h) JJASON 18 UTC.

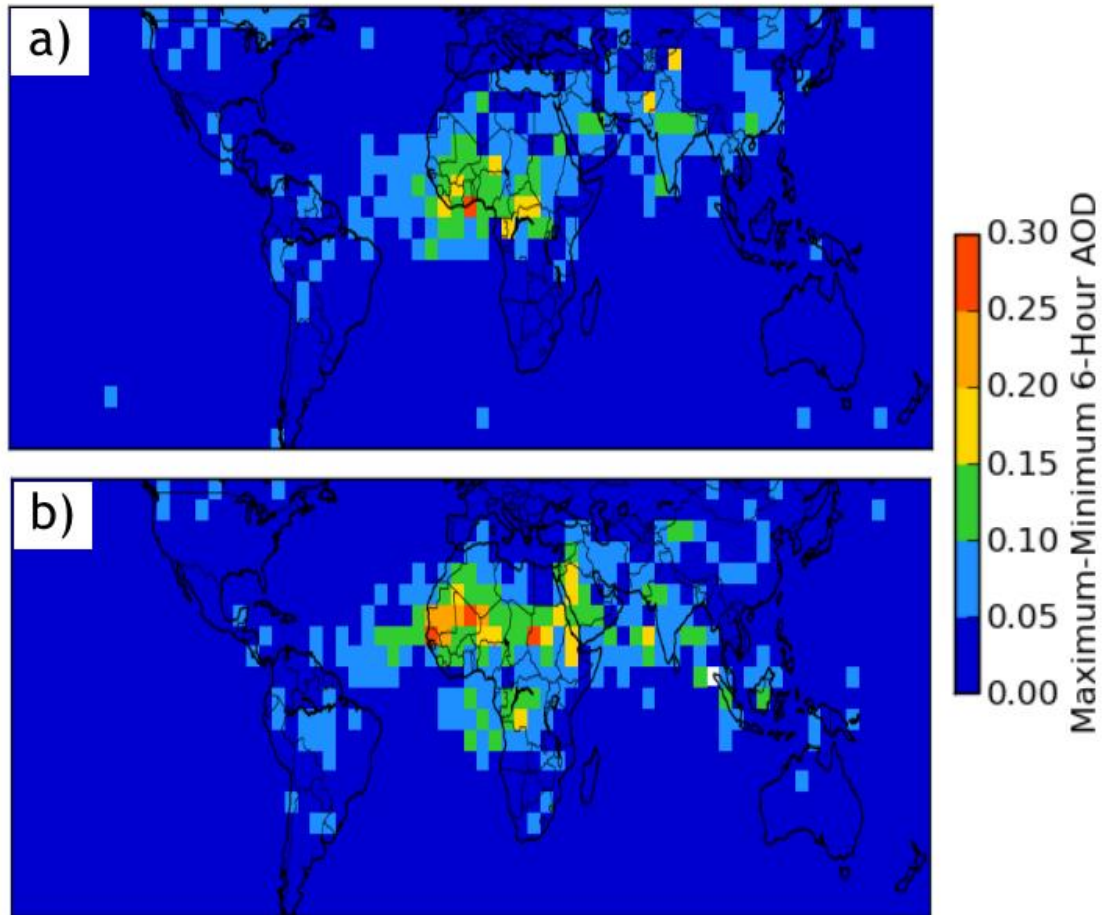
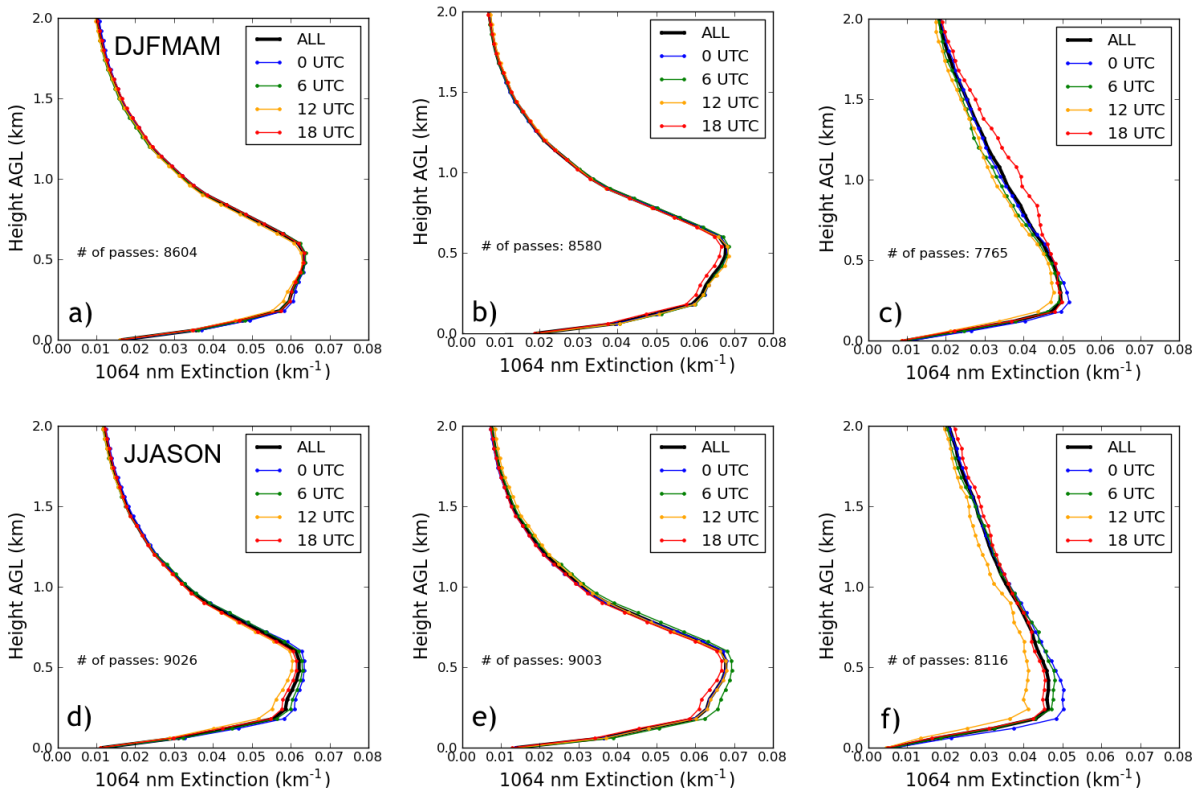


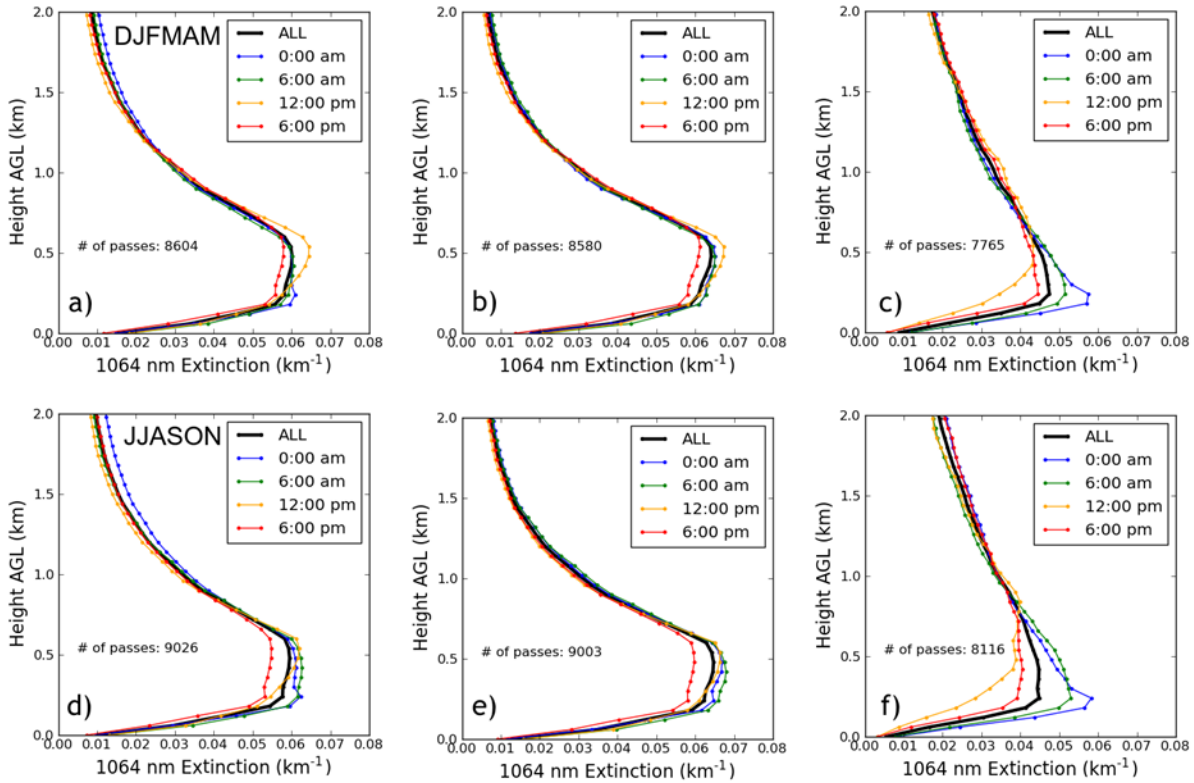
Figure 9. Maximum minus minimum mean seasonal AOD (1064 nm) for a) DJFMAM, and b) JJASON.



852

853

Figure 10. Global mean 6-hourly vertical profiles of CATS 1064 nm extinction for a) DJFMAM all profiles, b) DJFMAM water profiles, c) DJFMAM not-water profiles, d) JJASON all profiles, e) JJASON water profiles, f) JJASON not-water profiles. Mean AODs are as follows: a) 0.084, b) 0.078, c) 0.098, d) 0.089, e) 0.082, and f) 0.102.



855

856 Figure 11. Global mean 6-hourly local time (0:00 am, 6:00 am, 12:00 pm and 6:00 pm) vertical
 857 profiles of CATS 1064 nm extinction for a) DJFMAM all profiles, b) DJFMAM water profiles, c)
 858 DJFMAM not-water profiles, d) JJASON all profiles, e) JJASON water profiles, f) JJASON not-
 859 water profiles. Mean AODs are as follows: a) 0.080, b) 0.079, c) 0.095, d) 0.082, e) 0.081, and f)
 860 0.105.

859

860

861

862

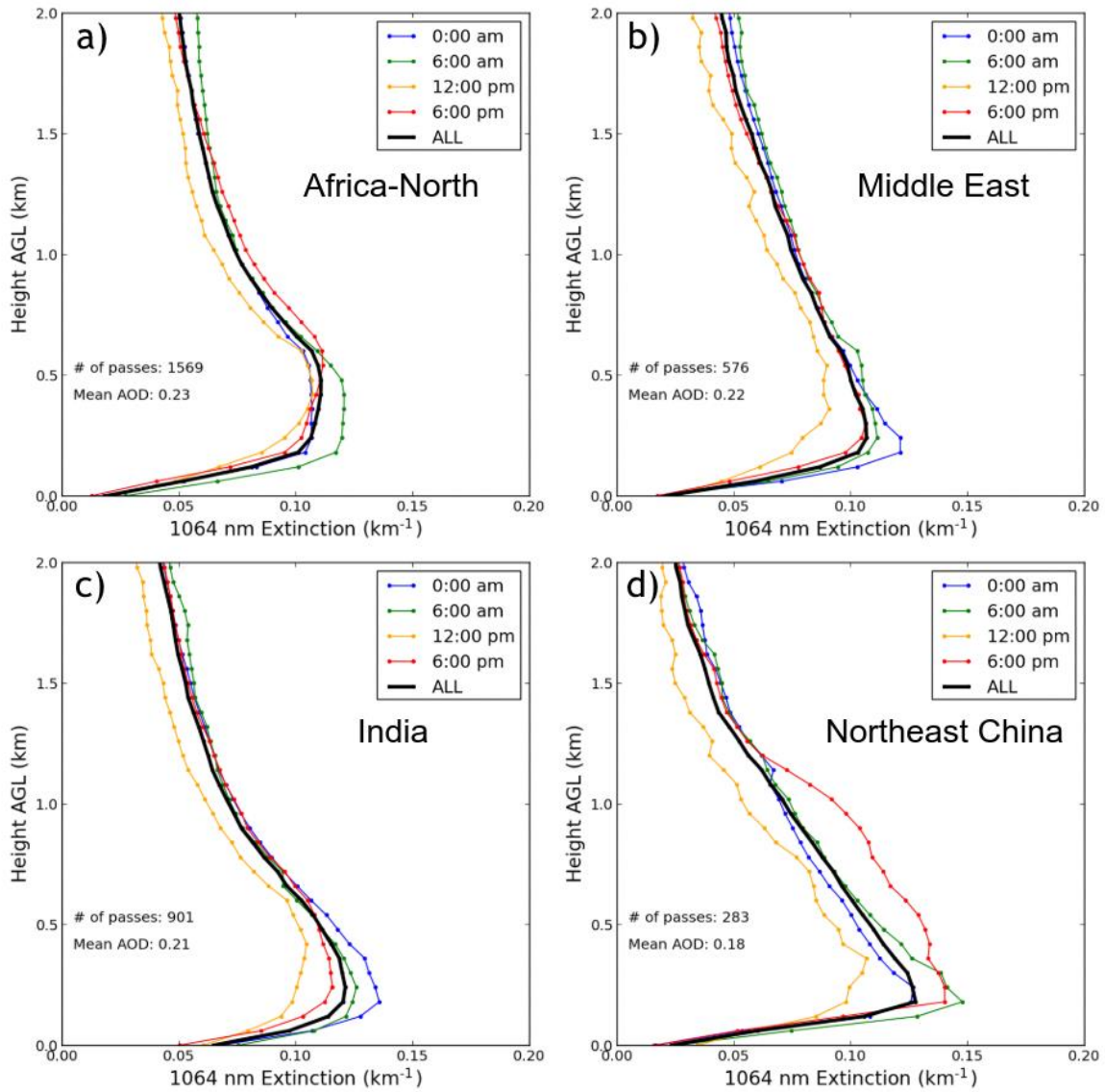
863

864

865

866

867



868

869 Figure 12. DJFMAM 6-hourly average (local time; 0:00 am, 6:00 am, 12:00 pm and 6:00
 870 pm) vertical profiles of CATS 1064 nm for locations shown in Figure 6a; a) Africa-North,
 871 b) Middle East, c) India, and d) Northeast China.

871

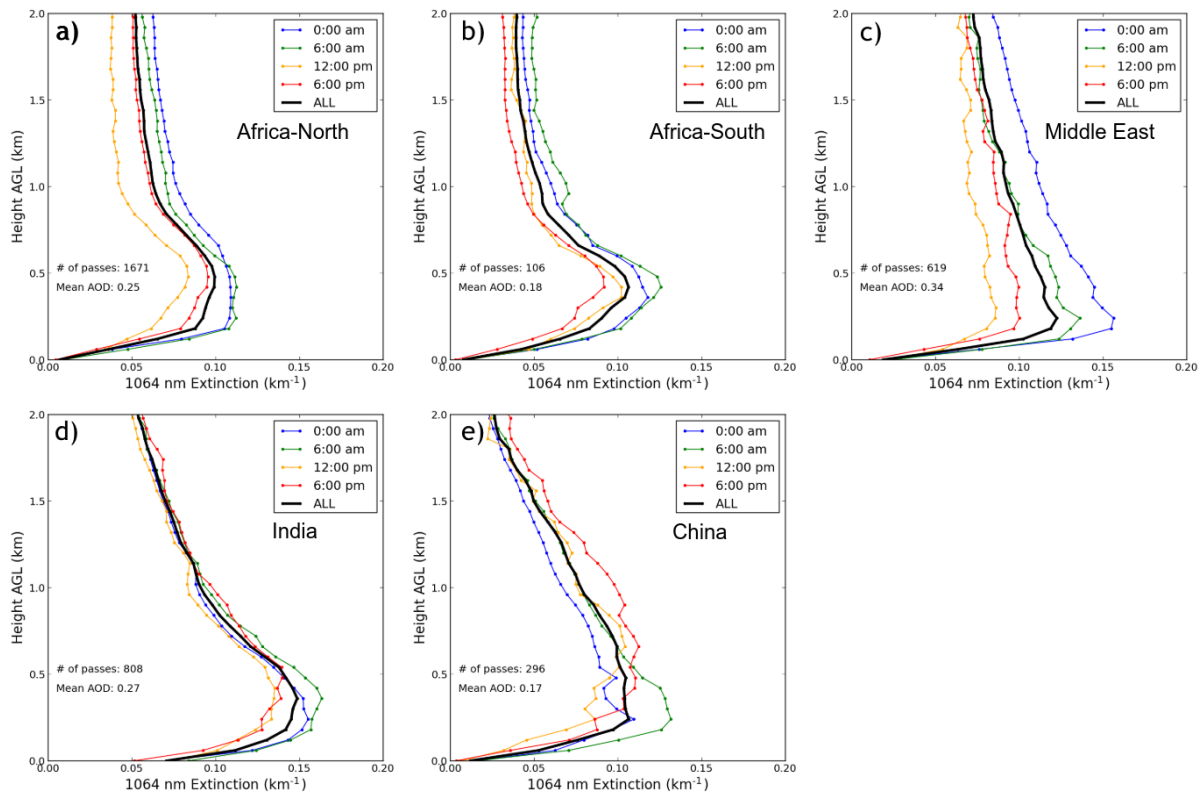
872

873

874

875

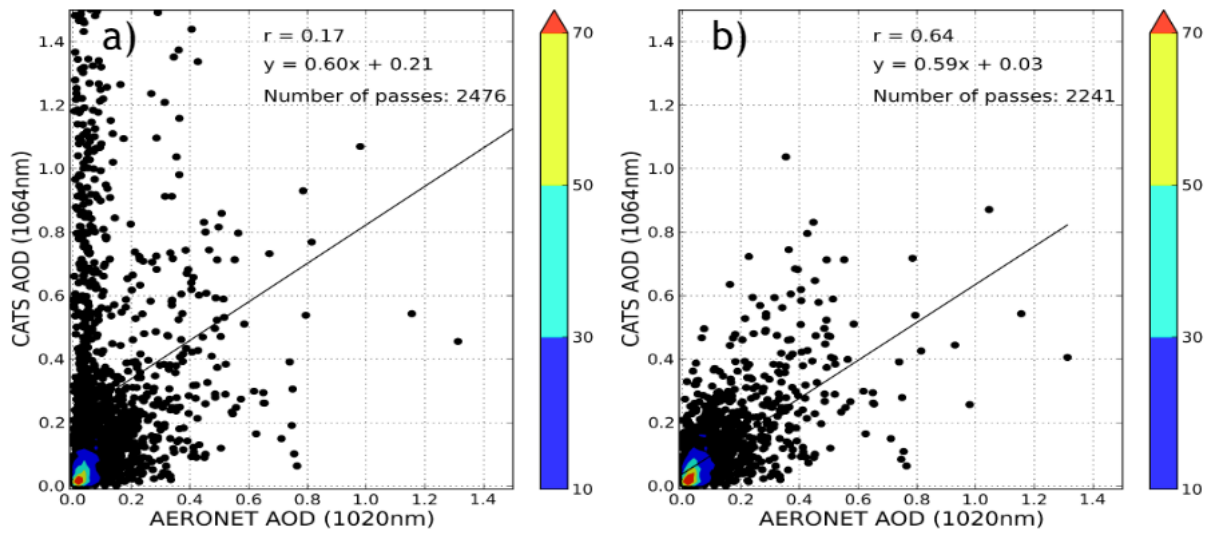
876



877

Figure 13. JJASON 6-hourly average (local time; 0:00 am, 6:00 am, 12:00 pm and 6:00 pm) vertical profiles of CATS 1064 nm for locations shown in Figure 6b; a) Africa-North, b) Africa-South, c) Middle East, d) India, and e) Northeast China.

878 Appendix A:
879



880
881
882
883
884
885

Figure A1. Collocated AERONET 1020 nm AOT vs. CATS 1064 nm AOD a) without CATS QA applied, and b) with CATS QA applied. CATS V2-01 aerosol products were used in constructing this plot.